**Title**

Mechanistic strategies of microbial communities regulating lignocellulose deconstruction in a UK salt marsh

**Authors**

Daniel R. Leadbeater[1§], Nicola C. Oates[1], Joseph P. Bennett[1], Yi Li[1], Adam A. Dowle[2], Joe D. Taylor[4], Juliana Sanchez Alponti[1], Alexander T. Setchfield[1], Anna M. Alessi[1], Thorunn Helgason[3], Simon J. McQueen-Mason[1§], Neil C. Bruce[1§]

[1] Centre for Novel Agricultural Products, Department of Biology, University of York, York, YO10 5DD, UK.

[2] Bioscience Technology Facility, Department of Biology, University of York, York, YO10 5DD, UK.

[3] Department of Biology, University of York, York, YO10 5DD, UK.

[4] School of Chemistry and Biosciences, University of Bradford, Bradford, West Yorkshire, BD7 1DP, UK.

[§] Corresponding authors: N.C.B. (email: neil.bruce@york.ac.uk), S.J.M.-M. (email: simon.mcqueenmason@york.ac.uk) or D.R.L. (email: daniel.leadbeater@york.ac.uk).

**Abstract**

**Background**

Salt marshes are major natural repositories of sequestered organic carbon with high burial rates of organic matter, produced by highly productive native flora. Accumulated carbon predominantly exists as lignocellulose which is metabolized by communities of functionally diverse microbes. However, the organisms that orchestrate this process and the enzymatic mechanisms employed that regulate the accumulation, composition and permanence of this carbon stock is not yet known. We applied meta-exo-proteome proteomics and 16S rRNA gene profiling to study lignocellulose decomposition *in situ* within the surface level sediments of a natural established UK salt marsh.

**Results**

Our studies revealed a community dominated by *Gammaproteobacteria, Bacteroidetes* and *Deltaproteobacteria* that drive lignocellulose degradation in the salt marsh. We identify 42 families of lignocellulolytic bacteria of which the most active secretors of carbohydrate active enzymes were observed to be *Prolixibacteracea, Flavobacteriaceae, Cellvibrionaceae, Saccharospirillaceae, Alteromonadaceae, Vibrionaceae* and *Cytophagaceae.* These families secreted lignocellulose-active glycoside hydrolase (GH) family enzymes GH3, GH5, GH6, GH9, GH10, GH11, GH13 and GH43 that were associated with degrading *Spartina* biomass. While fungi were present, we did not detect a lignocellulolytic contribution from fungi which are major contributors to terrestrial lignocellulose deconstruction. Oxidative enzymes such as laccases, peroxidases and lytic polysaccharide monooxygenases that are important for lignocellulose degradation in the terrestrial environment were present but not abundant, while a notable abundance of putative esterases (such as carbohydrate esterase family 1) associated with decoupling lignin from polysaccharides in lignocellulose was observed.

**Conclusions**

Here, we identify a diverse cohort of previously undefined bacteria that drive lignocellulose degradation in the surface sediments of the salt marsh environment and describe the enzymatic mechanisms they employ to facilitate this process. Our results increase the understanding of the microbial and molecular mechanisms that underpin carbon sequestration from lignocellulose within salt marsh surface sediments *in situ* and provide insights into the potential enzymatic mechanisms regulating the enrichment of polyphenolics in salt marsh sediments.

**Keywords**

Salt marsh, Lignocellulose, CAZyme, Carbon cycling, Carbohydrate esterase, CE1, Proteomics, Transcriptomics, Community profiling

## Introduction

Salt marshes are highly productive intertidal ecosystems that generate an abundance of organic carbon in the form of lignocellulose, where net aerial primary productivity often exceeds 1-2 kg C $m^{-2}$ $y^{-1}$ [1-3]. This productivity is intrinsically linked to organic carbon burial rates, estimated to be 57-245 g C $m^{-2}$ $y^{-1}$ [4-6]. This indicates that salt marshes are among the most effective carbon sequestering ecosystems per unit area on the planet with a total estimated sequestration capacity of 4.8 to 87.2 Tg C $y^{-1}$ [7] despite occupying only 22 000-400 000 $km^2$ [6-8]. These processes contribute to an increasing pool of inaccessible carbon as the salt marsh accretes. Organic carbon is introduced into the ecosystem as grass lignocellulose which represents the major component of surface to shallow sub-surface level carbon [9]. Furthermore, the composition of organic carbon changes with depth, with an enrichment in persistent lignin derivatives while polysaccharides are lost [10, 11]. Deposited lignin is subject to passive leaching of soluble and often biologically available phenols which diffuse throughout the sedimentary column, adding further recalcitrance to the remaining phenolics, degradation of which is suppressed in anoxic conditions [12-14]. Traditionally, primary productivity, surface area, sediment deposition and transport rates, leaching and sorption govern carbon capture in coastal sediments [15]. Mineral protection and preferential retention of recalcitrant organic carbon are major themes governing carbon sequestration [16]; however, throughout this natural biogeochemical carbon processing, microbial mechanisms of carbon transformation are present and likely operate as a system-level decomposition process that influences the permanence of lignocellulose and stored carbon in marsh sediments. Currently, this process is orchestrated by an undefined consortium of organisms prior to entry into stable deeper sediments where this material persists for millennia [6, 17].

Lignocellulose is a strong fibre composite material which provides mechanical support and the vessels for long distance water transport in plants, and is highly resistant to degradation. It is a macromolecular complex formed from cellulose microfibrils embedded in a matrix of branched polysaccharides known as hemicellulose. This polysaccharide complex is interpenetrated and sealed

by lignin, a phenolic heteropolymer, making lignocellulose more hydrophobic and difficult to degrade enzymatically [18]. The sheer abundance of lignocellulose in the terrestrial biosphere, along with its complexity and recalcitrance to digestion has led to the evolution of a diverse range of lignocellulolytic enzymes across the tree of life [19]. Yet very little is known about the factors that regulate lignocellulose decomposition in salt marshes despite large annual inputs into these systems as microdetritus that is predominantly retained and degraded on site [9, 20, 21].

The dominant flora in salt marsh ecosystems are perennial such as *Spartina* species. Dieback of these plants introduces vast quantities of lignocellulosic biomass into the marine environment. The first phase of decay occurs during dieback where terrestrial fungal plant pathogens, usually mycelial *Ascomycetes*, attack the senescent plant biomass [22, 23]. These fungi target standing senescent tissue that resides above-ground in a terrestrial setting and act to break open the plant cell walls as a means to access the nutritionally rich cell contents leading to the resultant infected tissues becoming nitrogen depleted and lignocellulose enriched [24-26]. The senescent standing tissue then weakens, and the lignocellulose enriched biomass detaches from the root-rhizome becoming deposited onto the sediment surface where it transitions into a predominantly marine environment with significantly greater and more variable physico-chemical pressures than terrestrial zones [27]. Here, it redistributes around the salt marsh surface or aggregates on the strandline where it is subject to a different phase of decay.

Studies have established degradation rates of deposited lignocellulose *in situ* at surface levels using litterbag methodologies [9, 20, 28-31], however; very little is known about the microbial framework that regulates this decomposition or the enzymatic mechanisms employed to deconstruct the complex lignocellulosic substrate. *In vitro* studies have suggested that bacteria, such as *Cyclobacteriaceae*, *Desulfobacteraceae*, *Flavobacteriaceae*, *Halomonadaceae*, *Oceanospirillales* *Pseudomonadaceae* and *Spirochaetaceae* are involved in lignocellulose degradation in this environment with fungi becoming competitively displaced [32-34]. Beyond this, our understanding

of the functional groups involved in the decomposition process and the biocatalytic strategies they employ to achieve this are poorly understood. *In vitro* studies are divorced from environmental factors and the findings require cautious interpretation, as results cannot be directly extrapolated into the context of ecosystem processes. Additionally, the function of an organism cannot be determined by its presence or the presence of a gene as this only deduces a potential propensity to function.

Direct monitoring of ecological processes *in situ* has the potential to capture functional, molecular and phylogenetic information at their environmental interface. To identify the microbial community that regulate the initial decomposition of introduced lignocellulose at the surface level, we applied meta-exo-proteome proteomics, ribosomal 16S rRNA gene phylogenetic profiling and lignocellulose composition analysis to *Spartina anglica* biomass in litterbags *in situ* along a 300 m transect within an established salt marsh (Welwick, UK) for 16 weeks (Figure 1, Additional file 1: Figure S1). We identify lignocellulolytic enzymes from the meta-exo-proteome, ascertain the taxonomic origin to identify functional groups and determine the mechanistic strategies they employ to depolymerize lignocellulose.

## Materials and Methods

### Experimental design

The field experiment was conducted in Welwick salt marsh, Hull, Humber estuary, UK, 53°38'55"N, 0°01'19"E from 16/7/15 to 6/11/15 (Additional file 1: Figure S1). To mimic natural lignocellulose cycling, senescent above ground *Spartina anglica* biomass was collected prior to deposition during winter dieback in February-March 2015 on an adjacent intertidal mud flat (Cherry Cobb sands, Humber estuary, Hull, UK). The biomass was washed free of sediment, dried at 65$^{o}$C for 48 hours and size fractionated with a Retsch Cutting Mill SM 300 at 2300rpm. The final biomass fraction consisted of 80% of >1.12mm fraction and 20% <1.12mm - >500µm fraction. Nylon 66

monofilament woven bags ('litterbag') (18.5cmx18.5cm) of aperture size 200µm were filled with 50g of biomass and sealed with 100% polyester thread.

Bags were placed in a 3 x 3 conformation in five stainless steel cages (711.2mm x 711.2mm x 63.5mm) with 25cm legs that were interspersed by 75m along a 300m parallel elevation transect, defined by plant zonation patterns (dominance of *Spartina anglica, Puccinellia maritima* and *Salicornia europaea*). Prior to deployment, the under canopy was removed and the cages placed with the bags interfacing with the sediment to facilitate crosstalk to mimic surface-interfacing detritus and mapped to position with GPS coordinates (Additional file 1: Table S1).

Sampling was performed by removing a single litterbag from each cage. During deployment, the uppermost 1-5mm of sediment surrounding the cages were sampled to act as a non-lignocellulose enriched sediment day 0 outgroup control. Sampling was randomised *a priori* and occurred weekly for the first six weeks and thereafter at week eight, ten and 16 for a total of 46 samples (including the day 0 outgroup). Sampling began at the point of low tide and was completed within two hours. Sampled bags were kept at 4$^{o}$C during transport and processing began within four hours of harvest.

**DNA and RNA extraction**

Each biological replicate at each time point (week one-six, eight, ten and 16) were treated independently. Harvested biomass was equilibrated twice with 40mL ice cold 0.5x PBS pH 8.15 and centrifuged for 10 min at 4500 xg. Five 0.5g biomass aliquots per litterbag (per cage; 25 total per week) were taken forward for DNA and RNA extraction. The five 0.5g biomass aliquots were added to screw cap tubes (2mL) containing 0.5g 0.5mM glass beads (Sigma G9268) and 0.5g 0.1mM glass beads (Sigma G8893). Cetyl trimethylammonium bromide buffer (0.5mL) containing 10% CTAB (m/v) in 0.7M NaCl, 240mM potassium phosphate pH 8 and 0.1% ß-mercaptoethanol and 0.4mL phenol/chloroform/isoamyl alcohol (25:24:1) pH 8 were added. The samples were homogenized in a

TissueLyser II (Qiagen) for 2 x 2.5 min at 30/s. The tubes were then centrifuged at 4°C at 16500g for 15 min. The aqueous phase was transferred to a new tube and an equal volume of chloroform:isoamyl alcohol (24:1) was added and centrifuged as previously and three 7.5g aliquots of decaying *Spartina* biomass per litterbag (one litterbag per each of the five cages for a total of 15 aliquots per week; only for weeks one, three, five and ten) were taken forward for protein extraction following Alessi *et al*. [35] The aqueous phase was precipitated for 16 hours at 4°C with two volumes of PEG precipitation solution containing 20% (w/v) PEG8000 (Sigma) in 1.6M NaCl. The nucleic acid pellet was collected by centrifugation as above for 30 min at 4°C. The pellet was washed twice in 75% ethanol. Total RNA from weeks one, three, five and ten (the same samples used to extract the proteins within the meta-exo-proteome) were taken forward for metatranscriptomic processing.

**Meta-exo-proteome extraction**

Each biological replicate in the protein extraction was treated independently. Per week, for each of the five cages, three aliquots (only for weeks one, three, five and ten, the same weeks utilised for metatranscriptome extraction to generate complimentary paired-in-time databases) were taken forward for protein extraction to generate meta-exo-proteome libraries. Each 7.5g aliquot of harvested biomass was washed twice with 40mL ice cold 0.5x PBS pH 8.15 and centrifuged for 10 min at 4500g. The extracellular and transmembrane proteins were labelled in triplicate and 2.5g biomass aliquots for each of the biological replicates were resuspended in 10mM EZ-link-Sulfo-NHS-SS-biotin (Thermo Scientific #21331) in 0.5x PBS and incubated at 4°C for 1 hour. The biomass was centrifuged for 10 min at 4500g as above, the supernatant was discarded and the biotinylation reaction was quenched with 25mL 50mM Tris-HCl pH 8 and incubated for 30 min at 4°C. Excess Tris-HCl and residual biotin was removed with two washes with 20mL ice cold 0.5X PBS pH8 with centrifugation steps for 5 min at 4500g.

Proteins were extracted from the biomass with 10mL 2% (w/v) SDS pre-heated to 60°C and incubated for 1 hour. The supernatant was extracted, and the proteins were precipitated with five volumes of pre-chilled (-20°C) 100% acetone and incubated at -20°C for 16 hours. Precipitated proteins were pelleted by centrifuging at 4500rpm for 20 min and the residual acetone was discarded. The pellets were air dried and resuspended in 1mL 0.1% SDS in 1x PBS, filtered through 0.22µm syringe driven filter units and loaded onto 1mL HiTrap Streptavidin HP columns (GE Healthcare #17-5112-01) and incubated for 1 hour at 4°C. The proteins were eluted with 1mL 50mM dithiothreitol (DTT) in 1x PBS, the column was incubated for a further 1 hour and eluted again, this was performed three times and the first two 1mL fractions were pooled.

The protein fractions were desalted, and buffer exchanged into $H_2O$ using 5mL Zeba™ Spin 7k MWCO columns (Thermo 89882) according to the manufacturer's protocol. To concentrate, the buffer exchanged protein was frozen in liquid nitrogen, lyophilized using a Heto PowerDry LL3000 Freeze Dryer (Thermo) and resuspended in 210µL $H_2O$. All five biological replicates for each time point were pooled in equal concentrations. The proteins were stored for LC-MS/MS analysis by solubilizing in NuPAGE LDS sample buffer (Life Technologies) and incubating at 70°C for 10 mins prior to a short (6 min) run into a 7 cm NuPAGE Novex 10% Bis-Tris Gel (Life Technologies) at 200 V. The gels were stained with SafeBLUE protein stain (NBS biologicals) for 1 hour before de-staining with $H_2O$ for 1 hour. The stained gels were sliced into $1mm^2$ fragments and stored at -20°C prior to LC-MS/MS analysis.

**Meta-exo-proteomics, protein identification, functional annotation and taxonomic origin**

To generate paired-in-time reference metatranscriptome databases, total extracted nucleic acids from each biological replicate were pooled in equal ratios for each time point (week one, three, five and ten) and DNA depleted. Messenger RNA (mRNA) was enriched by depleting ribosomal RNA

(rRNA) using Ribo-Zero™ Magnetic Epidemiology rRNA removal kit (RZE1224/MRZ11124C; Illumina). RNA-seq libraries were prepared using a NEBnext RNA Ultra Library preparation kit with NEBnext single 6bp indexing primers (New England BioLabs, Herts, UK) and pooled in equimolar ratios. The pooled RNA-seq library was spiked with 1% PhiX and sequenced on a single lane of an Illumina HiSeq 3000 2 x 150 base pair chip. Sequencing resulted in 82 966 97, 99 319 32, 95 318 91 and 105 517 252 raw reads for the metatranscriptomics databases for week one, three, five and ten respectively (383,122,461 reads in total); statistics for the four individual metatranscriptomic databases and totals are available in Additional file 1: Table S2.

To leverage the depth of sequencing and capitalise on the diversity within the temporally interspersed metatranscriptomes maximise protein identification, the metatranscriptomic databases for week one, three, five and ten were concatenated into a single master metatranscriptome. Raw reads were searched against Silva_115 database to identify ribosomal RNA (rRNA) genes using the Bowtie2 software package [35, 36]. Orphan reads in the paired reads, rRNA reads and poor quality sequences were removed with the ngsShoRT software [37]. Dereplicated libraries were assembled *de novo* with the Trinity software package [38]. Read counts and gene abundance were obtained with the Trinity utility programs. The *de novo* assembled metatranscriptomic databases contained 29 938 868 contiguous sequences (contigs). Contigs ≤500bp were filtered, split into open reading frames (ORFs) using Emboss GETORF (http://www.bioinformatics.nl/cgi-bin/emboss/getorf) that were ≥300bp and includes alternative initiation codons and dereplicated resulting in 2 400 360 unique ORFs within the master metatranscriptome.

To generate paired-in-time exo-meta-proteome databases, biological replicates at week one, three, five and ten were pooled and protein identification was performed in triplicate for each pool at each time point (N=3 for each of week one, three, five and ten). Tryptic digestion was performed for in-gel proteins post reduction with DTE and *S*-carbamidomethylation with iodoacetamide. Gel pieces were washed twice with 50% (v:v) aqueous acetonitrile containing 25 mM ammonium

bicarbonate and finally washed with acetonitrile and then dried. Modified porcine trypsin (Promega, Southampton, UK) was dissolved in 50 mM acetic acid and diluted with 25 mM ammonium bicarbonate to 0.02 µg/µL. 25 µL of trypsin solution was added and incubated for 10 min before adding 25 mM ammonium bicarbonate to submerge to gel pieces and incubated further for 16 hours at 37$^{o}$C. Three washes were performed with 50% (v:v) aqueous acetonitrile containing 0.1% TFA (v:v), dried and reconstituted in aqueous 0.1% trifluoroacetic acid (v:v).

The acquisition of peptide spectra was performed in triplicate for each time point and was achieved using a nanoLC system interfaced with a maXis HD LC-MS/MS system and a CaptiveSpray ionisation source (Bruker Daltonics, Coventry, UK). Positive ESI-MS and MS/MS spectra were acquired using AutoMSMS mode. Instrument control, data acquisition and processing were performed using Compass 1.7 software (microTOF control, Hystar and DataAnalysis, Bruker Daltonics). Instrument settings were: dry gas; 3 L/min, ion acquisition range; *m/z* 150-2 000, MS/MS spectra rate; 5 Hz at 2 500 cts to 20 Hz at 250 000 cts, quadrupole low mass; 300 *m/z*, cycle time; 1 s, ion spray voltage; 1,450 V, collision RF; 1,400 Vpp, transfer time; 120 ms, MS spectra rate; 5 Hz, dry gas temperature; 150°C, absolute threshold 200 counts, preferred charge states: 2–4, singly charged ions excluded. A single MS/MS spectrum was acquired for each precursor and former target ions were excluded for 0.8 min unless the precursor intensity increased fourfold.

Our approach of shotgun LC-MS/MS-based proteomics allows in-depth proteomic analysis, but is only effective if the peptide spectra can be matched to a corresponding sequence database. Because the salt marsh environment has been little explored at the molecular level, we used the metatranscriptome libraries, that were generated at the same time points (paired-databases in time) as the proteomic studies, as reference libraries to map peptide spectra to their originating sequence. We concatenated the four metatranscriptomic databases (week one, three, five and ten) into a master databases to capitalise on the diversity within the temporally interspersed metatranscriptomes and used this gene expression data to identify meta-exo-proteome proteins

from peptide spectra, shedding new light on the communities of microbes in this environment and their activities.

To identify proteins from LC-MS/MS spectra, peptide spectra generated from the digested meta-exo-proteome proteins were mapped back to originating sequences in the ORF library generated from the concatenated metatranscriptomic assemblies. Firstly, redundant sequences in the ORF database were removed by leveraging non-redundant sequences in an initial round of high stringency searching (p=0.05) against 21 subsets of ~115 000 sequences (252 searches total), followed by the concatenation of sequence hits into a secondary 'true hit' database (containing 42 894 sequences) with minimal redundancy, the final search against the true hit database (p=0.1) yielded 11,268 unique proteins; individual peptide spectral matches were filtered to require expect scores of 0.1 or better. Peptide spectra generated with LC-MS/MS were cross referenced with ORF sequences using Mascot version 2.5.1 (Matrix Science Ltd.), through the ProteinScape interface version 2.1 [39]. The search criteria for both searches were +2/+3/+4 peptide charge, peptide tolerance ± 10ppm, modifications; carbamidomethyl and oxidation. Analysis was performed using the quantitative exponentially modified protein abundance index (emPAI) [40]. emPAI values for each protein were then normalized to generate the molar percentage.

dbCAN was used to identify carbohydrate active enzymes (CAZyme) within the meta-exo-proteome and the metatranscriptomic databases using HHMER3 [41]. The meta-exo-proteome was also searched against the NCBI non-redundant protein database (NR_prot; 1:62) using BLAST+ (BlastP) version 2.2.31 with an expect value threshold of $1e^{-5}$ [42]. The resulting best-hit was obtained for each protein in the meta-exo-proteome and NCBI Accession and TaxID database was compiled and the most likely taxonomic origin of these proteins were established using tools within the Environment for Tree Exploration (ETE) version 3 toolkit [43]. To delineate functional members of the microbial community associated with the *Spartina* biomass, we cross-referenced the 16S rRNA gene phylogenetic profile with the taxonomic origin of the meta-exo-proteome proteins.

277

278 **16S rRNA gene and ITS2 amplicon sequencing and analyses**

279 Biological replicates were treated independently (N=5) for each of the 9 time points (week one-
280 six, eight, ten, 16 and the day 0 outgroup for a total of 46 data points). Total extracted nucleic acids
281 were RNAse A treated in triplicate. The ribosomal 16S rRNA gene V4 region was targeted with
282 primers; 515f-Y GTGYCAGCMGCCGCGGTAA (5'-3') [44] and 806R GGACTACNVGGGTWTCTAAT (5'-3')
283 [45]. The internal transcribed region 2 (ITS2) region was targeted with primers; fITS7
284 GTGARTCATCGAATCTTTG (5'-3') [46] and ITS4ngs TCCTSCGCTTATTGATATGC (5'-3') [47]. Cluster
285 identification was enhanced with a random dodecamer sequence NNNHNNNWNNN (5'-3')
286 prepended to the forward primer [48].

287 16S rRNA gene polymerase chain reactions (PCR) were performed in 25µL volumes containing
288 200µM dNTPs, 0.5µM 515fY-MN, 0.5µM 806rMN, 50ng gDNA, 0.5U Phusion HF polymerase
289 (#M0530) and 1x Phusion HF Buffer. Thermocycling conditions included an initial denaturation at
290 98$^{o}$C for 30s, followed by 28 cycles of 98$^{o}$C for 10s, 53$^{o}$C for 30s and 72$^{o}$C for 15s and 72$^{o}$C for 10
291 min. ITS2 PCR were performed as above with thermocycling conditions including an initial
292 denaturation at 98$^{o}$C for 30s, followed by 34 cycles of 98$^{o}$C for 10s, 57$^{o}$C for 30s and 72$^{o}$C for 20s,
293 with final extension at 72$^{o}$C for 5 min. Indexing was performed using the Nextera XT™ library
294 preparation kit (Illumina FC-131-1001). The libraries were pooled in equimolar concentrations to
295 4nM, spiked to 1% PhiX and run on a MiSeq 250bp x 2 cartridge (MiSeq Reagent Kit v2 (500 cycles)
296 MS-102-2003, Illumina).

297 The generated 16S rRNA genes libraries averaged 54,929 sequences. Fastq merging was
298 performed with Vsearch version 1.11.1 [49]. The generated ITS2 libraries averaged 50,843
299 sequences and were processed with ITSx [50] to filter non-fungi sequences. The resulting fungi only
300 ITS2 libraries averaged 28,972 sequences. The primer sequences were trimmed using Cutadapt
301 (version 1.11.). Sequences were trimmed to global lengths of 250bp using Usearch (version 9; -

fastx_truncate) [51]. Amplicon profiles were dereplicated, purged of singletons, assigned abundance and sorted by size using Usearch (version 7: -derep_fulllength) [51]. Clustering was performed using the UPARSE algorithm [52], with concurrent *de novo* chimera detection using Usearch (version 9 - cluster_otus) with a 97% identity threshold resulting in 5122 non-chimeric OTUs that were taken forward for analysis. Representative sequences for each OTU were then mapped to original sequences using Usearch (version 7: -usearch_global). Taxonomy was assigned with QIIME [53] (version 1.9; assign_taxonomy.py) using SILVA 132 [35] for the 16S rRNA libraries and UNITE v7.1 [54]. Rarefaction analysis [53] displayed curves that begin to reach asymptotic levels, indicating sufficient depth for analysis but not complete diversity coverage (Additional file 1: Figure S2). The taxonomy of any unassigned OTUs (N=610), using UNITE in the ITS2 libraries were further classified using BLASTn against the GenBank non-redundant nucleotide database. Non-fungal OTUs were discarded (N=) and missing taxonomies of on target OTU sequences were manually curated (N=393) resulting in a total of 920 fungal OTUs which were subsequently analysed. Fungal OTUs were classified into functional guilds using FUNGuild [55] which assigned a functional guild to 419 OTUs from 724 matches of the original 920, this represented 51.4 ± 2.12% mean OTU abundance across all time points and was taken forward for analysis. All commands for the analysis pipeline are available in Additional file 1: Table S3.

**Determining highly productive groups**

A productivity index was used to elucidate taxonomic groups with disproportionately greater CAZyme production per unit abundance, given by $\log_{10}(\sum \bar{x}$ mol%/abundance). Disproportionately productive groups were determined as those with an index >0.3 in at least 1 observation.

**Network associations**

Network associations between meta-exo-proteome CAZyme classes and taxonomic classes were constructed by grouping annotated domains (≤ $1e^{-10}$) into CAZyme classes by average ∑ x̄ mol% across the entire time course and connecting these nodes to the taxonomic classes the domains originated from. Classes are presented by their mean ∑ x̄ mol% output. Taxa < 0.025 ∑ x̄ mol% with ≤ 5 edges (connections) and CAZyme classes < $1.25x10^{-3}$ ∑ x̄ mol% were filtered for clarity. Plots were generated with NetworkX [56].

**Biomass composition analysis**

Biomass was washed free of sediment through 100µm mesh with free flowing $dH_2O$. Total biomass was measured as the mass balance of lyophilised material. Ash was determined with 1g of biomass incubated 600°C for 24 hours. Matrix polysaccharides were measured using triflouracetic acid methodology [57]. Cellulose was subsequently determined using the Updegraff and Saeman hydrolysis [58, 59]. Lignin was measured as acetyl bromide soluble lignin [60] using a previously cited extinction coefficient of 17.75 for grasses [61].

**Statistics**

One-way ANOVAs and Tukey's HSD tests were performed using SciPy [62] and Scikit [63] respectively. All data were assessed for normality using the Shapiro-Wilk test. Statistical analyses were performed on non-normalised data.

**Results**

**Functional assignment of the meta-exo-proteome**

To identify the lignocellulolytic enzymes involved in biomass breakdown, we employed a metaproteomic analysis of extracellular proteins (meta-exoproteome), accomplished by an affinity tagging process using a membrane-impermeable biotinylation tag [64]. Because lignocellulose is an insoluble macromolecule, it generally has to be broken down by extracellular enzymes. Many of the enzymes involved adhere to the lignocellulose or the microbe, and the use of surfactants to extract them leads to cell lysis and contamination with intracellular proteins. The tagging approach avoids the problem of intracellular contaminants, allowing a focus on extracellular and cell surface proteins.

Annotation of the transcriptome revealed 103 CAZyme families ($\leq 1e^{-5}$ and transcripts per million (TPM) $\geq 1$) across 44,334 ORFs (excluding glycosyl transferases), the total proportion of CAZYmes across all transcriptomic databases was 429.27 ± 62.16 TPM (Additional file 1: Figure S3). Proteomic analysis identified 11,268 proteins within the meta-exo-proteome, of which 320 ($\leq 1e^{-10}$) were annotated as putative carbohydrate active domains (CAZyme) within 252 peptide matching ORFs across 81 CAZyme families. Families present within the metatranscriptomic databases that were absent from the meta-exo-proteomes were largely families not specific to lignocellulose degradation or families usually associated with core intracellular activities (AA6, CE14, GH32, GH57, GH73, GH92 and GH108) or CAZyme families containing enzymes with both intracellular and extracellular localisations (GH1, GH2, CE7) with the exception of a small subset of predominantly pectin-targeting CAZymes; CE2, CE7, CE8, CE12, CE15, GH28 and GH105 and AA4 (Additional file 1: Figure S3). Instead, the exo-meta-proteome predominantly consisted of pectin-targeting CAZYme families CE3, CE4, CE6, PL1, PL4, GH35 and GH43.

CAZyme homologs ($\leq 1e^{-10}$) represented only 0.72-0.99 mol% of the total meta-exo-proteome concordant with previous *in vitro* reports [65]. The meta-exo-proteome CAZyme profile revealed three dominant Euclidean clusters of temporally abundant classes which contain a diverse collection of activities (Figure 2c). Glycoside hydrolases (GH) were the most abundant class with 37 families identified. GH3, GH5 and GH6 family enzymes were abundant, these classes are typically related to

cellulose degradation, many of which were associated to carbohydrate binding domains (CBMs). The CBM profile of our data highlighted two abundant Euclidean clusters (Figure 2d); the dominant of which contained CBM2 and CBM44 motifs associated with cellulose and matrix polysaccharide binding and a secondary cluster containing CBM10, CBM5 and CBM60 which have been associated with cellulose, hemicellulose and chitin binding, respectively. Families associated with hemicellulose degradation were abundant, notably GH10, GH11 and GH16 typically associated with xylan degradation.

A rapid loss of dry mass was observed with a reduction of 69% during the 16 week period. The distribution of CAZyme family proteins coupled with the biomass composition revealed successional targeting of the major lignocellulose biopolymers (Figure 2a-b), that temporally synchronized with the abundance of CAZyme proteins within the meta-exo-proteome. The largest loss in cellulose occurs during the first week, most likely conducted by the highly abundant GH6 and GH5 family enzymes coordinated with CBM2 and CBM44 domains targeting exposed cellulose microfibrils generated as a result of the mechanical fractionation of the *Spartina anglica* biomass, while lignin degradation appears rate limiting (weeks one and two). During weeks three to five, there was an increased rate of matrix polysaccharide loss which corresponds to an increased abundance of GH11, GH10, GH13 and GH43 family enzymes coupled with a concomitant decline in the rate of cellulose hydrolysis, suggesting matrix polysaccharides limited cellulose access. During weeks 6 to 16, the rate of cellulose deconstruction increases and a degradative equilibrium was established.

An interesting finding was that carbohydrate esterases (CE) were more abundant than many GH family enzymes (Figure 2b), particularly those from family 1 (CE1) that predominantly presented as feruloyl esterases and acetyl xylan esterases. Auxiliary activities (AA) established largely as encompassing oxidative enzymes, while present within the enzymatic profile, were not abundant. We only identified two AA families; AA7 (glucooligosaccharide oxidases and chitooligosaccharide

oxidases) which were transiently present during week three and AA2 (containing class II lignin-modifying peroxidases) that were present at low abundances throughout the study.

**Taxonomic affiliation of meta-exo-proteome proteins**

Fungi and archaea were poorly represented in our metaproteome annotations and were only responsible for 0.28-1.46 and 0.04-0.2 mol% of the total meta-exo-proteome, respectively. Bacteria produced 99-100 mol% CAZymes. Indeed, within the CAZyme profile, the only notable proteins not of bacteria/archaea origin showed homology to Annelida (AA2) and Chlorophyta (AA3) enzymes. This was concordant with the total meta-exo-proteome, of which 66.5-79.5 mol% originated from bacteria/archaea.

Proteins that originated from families also identified in the 16S rRNA gene derived community profile accounted for 75 ± 6.9% CAZyme mol%. The results indicate *Proteobacteria* and *Bacteroidetes* are the dominant producers of lignocellulolytic enzymes (Figure 3a). *Gammaproteobacteria* and *Deltaproteobacteria* were responsible for 39.03 ± 13.65% and 7.48 ± 3.95% of total CAZyme mol%, respectively, while *Bacteroidia*, *Flavobacteriia* and *Cytophagia* were responsible for 12.45 ± 6.30%, 9.25 ± 2.55% and 7.45 ± 3.03% of the total CAZyme mol%, respectively. This is concordant with the 16S rRNA gene abundance of these two phyla, which is maintained at 78.43 ± 4.10%. Investigations revealed *Alteromonadaceae* (*Alteromonas, Rheinheimera and Catenovulum*), *Vibrionaceae* (*Vibrio*), *Flavobacteriaceae* (predominantly *Lutibacter, Wenyingzhuangia* and *Flavobacterium*), *Cellvibrionaceae*, *Saccharospirillaceae* and *Reinekea*, *Prolixibacteraceae* (predominantly *Draconibacterium, Prolixibacter* and *Sunxiuqinia*), *Marinilabiliaceae (Saccharicrinis)*, *Saccharospirillaceae* (*Reinekea*) and *Bacteroidaceae (Bacteroides)* as dominant CAZyme producers (Figure 3). Groups with disproportionately high CAZyme productivity relative to their abundance were revealed as *Bacteroidaceae* (*Bacteroides*), *Paludibacteraceae* (*Paludibacter*), *Flammeovirgaceae* (*Flexithrix*), *Sphingobacteriaceae*, *Melioribacteraceae* (*Melioribacter*),

*Chromatiaceae*, *Peptococcaceae* and *Salinivirgaceae* (*Salinivirga*) (Additional file 1: Figure S5). CAZyme productive but poorly resolved genera included *Teredinibacter, Sporocytophaga, Aquimarina, Hyunsoonleella, Planococcus, Pseudosphingobacterium, Desulfosporosinus, Formosa, Simiduia, Sorangium, Lentimicrobium, Arcticbacter, Desulfobulbus, Saccharophagus* and *Chitinophaga* (Additional file 1: Figure S4).

Fungi were identified within the sediment and lignocellulosic material but no CAZymes originating from fungi were detected. Significant changes in fungal OTU richness was observed (ANOVA, $F_{8,36}$ = 14.95, $p<2.29x10^{-9}$) with a significant increase (ANOVA, $F_{1,8}$ = 29.17, $p<0.0006$) between week one to the observed peak during week two from 253 ± 35 to 360 ± 18.54 respectively, before entering a gradual but continuous decline to week 16 (N=180 ± 24.2) (Additional file 1: Figure S11). Fungal taxonomy was poorly resolved with 558 of 920 OTUs identified to class level. Identified fungi were predominately *Ascomycetes* (56.38 ± 4.07%) with a small contribution from *Basidiomycota* (5.22 ± 1.57%; however, in the day 0 sediment *Rozellomycota*, *Chytridiomycota* and *Zygomycota* were observed as very minor components.

*Saccharomycetales* and *Pleosporales* were consistently abundant within the lignocellulose associated fungal community throughout the 16 week time course (25.6 ± 3.23% and 10.85 ± 1.74% respectively) (Additional file 1: Figure S11). Notable components of the early fungal profile included *Hypocreales*, *Capnodiales*, *Tremellales* (weeks one through to three) before rapidly declining and seemingly displaced by *Microascales* which enrich and dominate the profile between week five (1.82 ± 1.2%) and six onwards (10.2 ± 4.45%). Functional classification of these OTUs in terms of nutrient acquisition strategy revealed the dominant guild to be saprotroph, followed by pathotroph-saprotroph (Additional file 1: Figure S12), of which the most prevalent trophic modes were undefined saprotroph which enriched gradually from 32.3% in the day 0 sediment outgroup to 86.1 ± 3.32% at week 16, endophyte-lichen parasite-plant pathogen-undefined saprotroph which were consistent between week two to 16 (20.1 ± 1.91%) and animal pathogen-endophyte-lichen parasite-

447 plant-pathogen-soil saprotroph-wood saprotroph which was a large component only during weeks
448 one to three (13.8 ± 1.72%; Additional file 1: Figure S11), both of which are poorly resolved
449 definitions. Interestingly, modes associated with the turnover of lignocellulosic substrates such as
450 wood saprotroph and leaf saprotroph were more abundant in the day 0 sediment outgroup than in
451 the lignocellulose associated community.

452 Filtering out non-CAZyme productive lineages revealed a rapid enrichment for CAZyme producing
453 families relative to the day 0 sediment outgroup. This suggests that within the sediment a maximum
454 of 13.9% of the bacteria/archaea microbiome at family level functioned as lignocellulose degraders
455 whilst OTU richness was highest (2277). During the first week within the biomass, we observed an
456 enrichment in CAZyme productive lineages of 3.77 ± 0.11 fold to 52.40 ± 1.51% of the total
457 community whilst OTU richness declined (1020 ± 65), increasing to 59.56 ± 1.66% in week two
458 (Figure 3b-c). We observed significant variation in OTU richness over time (ANOVA, $F_{8,36} = 17.59$,
459 $p<0.000005$), increasing significantly from week one to three and all time points thereafter (Tukey
460 HSD, $p<0.015$). OTU richness continued to increase toward day 0 outgroup levels while no significant
461 decline in the abundance of CAZyme producing members was observed during the time course
462 (ANOVA, $F_{8,36} = 1.78$, $p>0.114$) suggesting the colonisation of diverse heterotrophs and secondary
463 metabolizers. Concordantly, the total CAZyme mol% was not significantly different throughout the
464 time series (ANOVA, $F_{3,8}= 1.06$, $p>0.42$).

465 We noted a degree of congruence between the enzymatic profiles of the most productive groups
466 within *Proteobacteria* and *Bacteroidetes* (Figure 4, Additional file 1: Figures S4-7). The most
467 abundant CAZyme classes (Figures 2c-b) with the exception of GH6, CBM2, CBM10 and CBM44 that
468 were produced exclusively by *Gammaproteobacteria*, represented a core suite of activities (Figure 4)
469 and were produced by multiple divergent lineages, suggesting a common mechanistic strategy was
470 employed by the major CAZyme-producing consortia (Figure 4).

*Gammaproteobacteria* maintain unparalleled levels of CAZyme production across the time course despite a reduction in their overall abundance. This is due to an enrichment in clades exhibiting high CAZyme production, e.g. *Alteromonadaceae*, *Saccharospirillaceae* and *Vibrionaceae.* *Cellvibrionaceae, Alteromonadaceae* and *Saccharospirillaceae* are not abundant in sediments but progressively became major components of the *Gammaproteobacteria* profile in both the community profile and their CAZyme output. *Vibrionaceae* appear transient with peak abundance during week one (22.98 ± 3.27%) which precedes a steady decline (5.25 ± 1.04% and 2.70 % ± 0.70% in weeks two and three, respectively), indicating that this clade represent rapid colonizers and opportunistic oligotrophs. *Vibrionaceae* was predominantly comprised of two genera, *Vibrio and Photobacterium.* Subsequently, *Vibrionaceae* appears to be outcompeted by *Alteromonadaceae*, *Saccharospirillaceae* (*Reinekea),* and *Cellvibrionaceae* (predominantly *Marinagarivorans)*; accounting for much of the decline in the *Gammaproteobacteria* profile in weeks one to five. Identifiable *Alteromonadaceae* genera included *Alteromonas, Glaciecola* and *Paraglaciecola.* *Gammaproteobacteria* abundance is supplanted by *Deltaproteobacteria* groups*; Desulfobulbaceae, Desulfuromonadaceae* and *Desulfovibrionaceae* and *Bacteroidetes* groups; *Prolixibacteraceae (Draconibacterium* and *Roseimarinus)*, *Flavobacteriaceae* (*Lutibacter*) *and Marinilabiliaceae* (*Labilibacter*). Families within *Firmicutes* and *Verrucomicrobia* were active CAZyme secretors despite low apparent abundances; particularly *Peptococcaceae*, *Planococcaceae* and *Paenibacillaceae and Rubritaleaceae.*

**Discussion**

We examined the process of surface level lignocellulose decomposition within a natural salt marsh environment demonstrating a framework wherein lignocellulose decomposition can be monitored *in situ*. Our data suggest a large proportion of the total native microbiome is lignocellulose responsive and capable of rapid colonization and restructuring to take advantage of this annual influx of carbon. Our metaproteomic studies revealed an enrichment for activities that

497 target linkages between lignin and polysaccharides as well as glycanohydrolases and a marked
498 sparseness of oxidative enzymes that attack lignin.

499 It is notable that although the total biomass in our mesh bags was reduced by about 70% over a
500 16 week period, our results conform to a first order decay model alluded to in previous experiments
501 [28, 66-68]. These previous studies suggest the majority of particulate decomposition occurs within
502 the first year of entry into the system and proceeds through three phases; the leaching of soluble
503 compounds, decomposition and a final refractory phase characterized by diminished rates of
504 decomposition [28, 66-68]. Valiela et al., [66] suggest the refractory period is confined to
505 decomposition rates below 0.4% $day^{-1}$. In our study, the decomposition rates for the refractory
506 period during weeks eight and 16 were observed to be 0.22 ± 0.087% $day^{-1}$ and 0.176 ± 0.03% $day^{-1}$
507 respectively, suggesting our experiment ran into the refractory period.

508 We assessed surface level, aerobic lignocellulose decomposition as it has been shown to be
509 significantly more efficient than sub-surface decay [30]. Valiela et al. [30] explored the relative
510 composition of *Spartina alterniflora* for 24 months beginning in winter. While the study findings are
511 not directly comparable to our own due to differing location, start date and species of biomass,
512 which significantly affects decomposition [68], there is an undeniable synchrony between the
513 profiles of lignocellulose degradation in both studies. Both studies demonstrated an initial increase
514 in cellulose and hemicellulose, sequentially followed by lignin degradation, then hemicellulose
515 degradation. The hemicellulose degradation then coincides with cellulose degradation whilst lignin
516 increases.

517 The relative enrichment in lignin, accepted as the most recalcitrant component of lignocellulose
518 [18], suggests this biopolymer is not actively targeted for metabolism by the microbial community.
519 Salt marsh sediments are known to be significantly enriched in lignin-derived high molecular weight
520 polyphenols, with these increasing in concentration with depth [10, 11, 30, 69]. Conversely, the
521 more biologically available polysaccharides reduce with depth as they are known to be preferentially

targeted [70-72]. As lignin interpenetrates the core polysaccharides in the lignocellulosic matrix it must be removed before the internal polysaccharides are accessible for digestion. Oxidative enzymes are the predominant mechanism exhibited in terrestrial systems to modify and degrade lignin, yet in our study only AA2 family members were present at low abundances. These enzymes attack lignin moieties to modify the structure and it is unlikely they are responsible for cleaving high molecular weight phenolics that are observed in salt marsh sediments. These findings suggest that native salt marsh organisms have enzymes responsible for lignin modification that are not yet known or that they adopt other mechanisms able to facilitate access to the valuable sugars present in lignocellulose.

Instead, we note that the salt marsh meta-exo-proteome has a high representation of carbohydrate esterases (CE), particularly from family 1 (CE1). CE1 family enzymes function non-oxidatively to remove cinnamoyl and acetyl esters from xylans, disrupting the lignin-carbohydrate complex interface between hemicellulose and lignin, and hemicellulose and cellulose respectively [18, 73]. Lignin-carbohydrate complex linkages are thought to consist mainly of aryl ester (from ferulic acid to arabinose in grasses like *Spartina anglica*) and aryl ether bonds, hydrolysis of which decouples the lignin, exposing the surface of the remaining polysaccharides [74]. The CE1 family includes a range of esterases, especially those which hydrolyse ester links between arabinoxylans and ferulic and coumaric acid residues. Ferulic acid residues in arabinoxylans are particularly important in providing linkages between arabinoxylan chains and between arabinoxylans and lignin, thereby contributing significantly to lignocellulose recalcitrance [18, 75, 76]. CE1 also contains xylan acetylesterases that remove acetyl groups from arabinoxylan, having major impacts on their three dimensional conformation and ability to bind cellulose [77]. Previous compositional analysis of decomposed lignocellulose in salt marshes have revealed trans-ferulic acid was responsible for 57-82% of the total lignin loss which agrees with the mechanism identified in our study [78]. This indicates that the linkages holding lignin to the polysaccharides of lignocellulose may be major targets to allow GHs access to their substrates. We contend that this mechanism is favourable within

548 salt marshes in contrast to terrestrial systems due to the liquid medium facilitating desorption of
549 dissociated lignin macromolecules into the surrounding waters, circumventing the requirement for
550 total deconstruction. This mechanism could explain the enrichment of persistent lignin-rich particles
551 known to accumulate in salt marsh sediments through the cleavage of high molecular weight
552 phenolics. These phenolics are then likely subject to oxidative modification by the low abundance
553 AA2 family enzymes causing them to slowly become biologically available.

554 Previous studies suggest lignocellulose degradation within sediments is driven by bacteria, which
555 is supported by our data [32, 34], yet fungi are known to populate salt marsh sediments but their
556 function, community ecology and interactions remain elusive [79]. We did identify a handful of
557 fungal families with potential historical connections to lignocellulose, predominantly *Pleosporaceae*,
558 *Hypocreaceae, Nectriaceae, Sordariaceae* and *Saccharomycetales* [80]. Nutrient acquisition
559 strategies of the identified fungi revealed the dominant trophic mode to be saprotroph (acquire
560 nutrients from dead organic matter) and to a lesser extent pathotroph (acquire nutrients by
561 attacking cells) and combinations thereof. This suggests most fungi were acquiring nutrients from
562 alternative dead organic matter or were utilising a pathotrophic acquisition strategy where
563 lignocellulose is not a primary target. A notable observation was that wood saprotrophs and leaf
564 saptrotrophs, which would be expected to thrive on the dead *Spartina* biomass which included
565 stems, leaves and sheaths, were present in the sediment but were not abundant on the
566 lignocellulosic material. As fungi are orders of magnitude less abundant than bacteria in this system
567 [81, 82] and we did not detect lignocellulolytic enzymes from these groups within the meta-exo-
568 proteome despite fungal enzyme sequences being well represented in archive databases, our data
569 would suggest their influence on lignocellulose decomposition for material within salt marsh
570 sediments is negligible and they likely target alternative sources of organic matter that are present
571 or cohabit within the lignocellulosic aggregate.

572 Bacterial families that have been implicated with salt marsh lignocellulose degradation based on
573 isotope probe experiments include *Desulfobacteraceae*, *Spirochaetaceae*, *Kangiellaceae* [32] and
574 selective enrichments include *Flavobacteriaceae*, *Cyclobacteriaceae*, *Pseudomonadaceae* and
575 *Halomonadaceae* [34]. We did not observe the groups reported by Darjany *et al*. [32] to be active
576 lignocellulose degraders, since the majority of lignocellulose deconstruction occurs within the
577 extracellular matrix the breakdown products are available to all microbes within proximity, therefore
578 the $^{13}C$ approach employed by Darjany *et al.* [32] possibly identified benefactors of breakdown
579 products rather than organisms actively degrading lignocellulose. We did identify all major groups
580 reported by Cortes-Tolalpa *et al.* [34] in our *in situ* study which confirm these groups to be active
581 secretors of lignocellulolytic enzymes. We also identified an additional 38 families that were not
582 previously known to actively secrete lignocellulose active enzymes. The 42 CAZyme producing
583 families reported here underpin long term carbon sequestration using a mechanism that appears to
584 favour the degradation of complex polysaccharides by selectively avoiding lignin degradation. This
585 process not only expands the pool of stored carbon but also reduces complex carbohydrates to
586 biologically available molecules within the extracellular space for the wider microbial community.

587 The CAZyme-producing *Gammaproteobacteria* described here appeared to be early colonizers of
588 lignocellulose that undergo taxonomic restructuring to favor heterotrophic lineages.
589 *Gammaproteobacteria* are displaced by CAZyme-producing groups belonging to *Bacteroidetes* and
590 *Deltaproteobacteria* clades. The results suggest the *Gammaproteobacteria* families are the
591 ecologically dominant surface level lignocellulose degraders. The divergent families identified within
592 *Bacteroidetes* and *Deltaproteobacteria* suggest they are highly active at surface levels, but likely
593 dominate carbon cycling in the oxygen depleted cores of biomass aggregates and in shallow to deep
594 subsurface sediments as they have been identified in abundance within deeper sediments. However;
595 their ecological functions were previously unknown [83].

Well studied examples of marine lignocellulolytic *Gammaproteobacteria* include *Saccharophagus degradans* and the closely related *Teredinibacter turnerae*, belonging to families *Alteromonadaceae* and *Cellvibrionaceae,* respectively. Both families were abundant within the lignocellulose responsive microbiome and identified to be highly productive of CAZymes and interestingly, neither family were well represented within the day 0 sediment outgroup suggesting they function as saprotrophs within the salt marsh. *S. degradans* is a well characterised free-living heterotroph that appears fully capable of deconstructing complex plant cell wall polysaccharides and many other biopolymers [84, 85]. The use of these bacteria as a source of enzyme cocktails for lignocellulose saccharification has been explored due to the broad complement of CAZymes [86] and full cellulolytic system [87]. Dominant CAZymes within *S. degradans* culture supernatant include GH3, GH5, GH6, GH9, GH10 and GH16 many of which are multi-domain with a prevalence of CBM2 and CBM10 containing proteins as well as CBM6, CBM13 and CBM32 [88], all of which collectively correspond to highly abundant *Gammaproteobacteria* associated CAZyme families identified within our exo-meta-proteomics.

*T. turnerae* is a facultative intracellular endosymbiont found in wood-boring bivalves, it is cellulolytic with demonstrated cellulose degrading capability and more recently it has been found to harbour a complex array of xylan degrading enzymes and lytic polysaccharide monooxygenases [89, 90], yet it possesses a relatively small repertoire of CAZYmes that only target woody plant biomass within its genome compared to *S. degradans* [91]. These are predominantly GH5, GH6 and GH11 that also include multi-domain proteins often associated with CBM5 and CBM10 domains that were well represented in our corresponding *Gammaproteobacteria* exo-meta-proteome [91-93]. The prevalence of multi-domain proteins containing CBMs, particularly within the cellulases, observed both within the well-characterised marine isolates and observed to be highly abundant within this study have been suggested to function as a tether as opposed to a catalytic enhancement [88]. Less than 40% of terrestrially derived cellulases contain CBMs that are conventionally thought to increase the effective concentration of enzyme at the substrate surface and therefore rates of activity [94]. In salt marshes, adsorption of CBM containing enzymes would act to tether and localise the enzyme to

622 the substrate, improving substrate beneficiation to the secretor by preventing them from being
623 washed away in these intertidal regions. It is possible that the predominance of CAZymes possessing
624 CBMs has facilitated the *Gammaproteobacteria* to flourish within the early stage of surface level
625 decomposition within the salt marsh as observed in both our exo-meta-proteome and independent
626 16S rRNA amplicon profile.

627 Carbohydrate active enzymes are an incredibly broad designation of enzymes that includes both
628 the intracellular and extracellular biosynthesis and breakdown of complex and simple
629 polysaccharides. Accurately determining extracellular localisations of proteins from transcripts,
630 particularly in an underexplored environment such as a salt marsh is challenging. Therefore, we
631 applied exo-meta-proteomics to accurately determine proteins existing within the extracellular
632 matrix. We successfully identified 81 CAZyme families within the exo-meta-proteome of the 103
633 identified within the metatranscriptome libraries suggesting sufficient depth of coverage of the
634 extracellular encompassing families. However, due to the salt marsh ecosystem being intertidal, it is
635 possible our analysis has not detected transiently localised enzymes. This may explain the small
636 subset of predominantly pectin-targeting CAZyme families that were present within the
637 transcriptome but not detected within the exo-meta-proteome as pectin is widely considered the
638 most soluble component of the plant secondary cell wall.

639 Our approach targeted the rapid surface level deconstruction phase of lignocellulose. While the
640 salt marsh microbiome varies marginally with elevation at the sediment surface [95], it is
641 significantly variable with depth [83]. These changes are a function of oxygen depletion, leaching
642 rates, sorption characteristics and alternative respiratory terminal electron acceptor availability.
643 Considered together with the relative enrichment in lignin derived polyphenolics [10, 11, 96, 97] this
644 suggests the lignocellulose-active community could be stratified with depth. These communities may
645 employ alternate mechanisms than identified here that target the most recalcitrant, lignin enriched
646 material that has once passed through the initial surface level decomposition phase we describe.

Our results only capture the initial rapid surface level decomposition phase, these findings cannot be extrapolated throughout the salt marsh sedimentary column where the majority of the carbon stock persists. Further exploration of the microbial communities at depth is required to elucidate the functional taxa and the mechanisms they employ to degrade the lignin enriched carbohydrate complexes that progressively accumulate and contribute to the extensive pool of sequestered carbon as substrate composition is known to modulate the mechanisms employed [98].

## Conclusions

Our study captured lignocellulolytic organisms as they functioned *in situ* at their environmental interface within surface sediments in a salt marsh. We identified 42 families that actively secrete enzymes that act to deconstruct lignocellulosic polymers, 38 of these families had no previously proven ecological function. Our data suggest that bacteria primarily orchestrate this process within sediments with no detectable contribution from fungi despite being present. Our proteomic analysis of the meta-exo-proteome highlighted *Gammaproteobacteria* as early lignocellulolytic colonisers that are temporally displaced by *Bacteroidetes and Deltaproteobacteria* groups and these taxa concurrently produce a core suite of diverse enzymes that act upon lignocellulose. This also revealed a potential mechanism of deconstruction, driven by carbohydrate esterase family 1 enzymes, which are capable of dissociating lignin macromolecules from the core polysaccharides within the lignocellulosic complex. This degradative strategy potentially explains the accretion of lignin derived polyphenolics within salt marsh sediments. As our study assessed early stage surface level degradation, further research is required to elucidate mechanisms that drive organic carbon storage and turnover in deeper sediments.

## Abbreviations

**AA:** Auxiliary activity enzyme

**CAZyme:** Carbohydrate-active enzymes

**CBM:** Carbohydrate-binding module

**CE:** Carbohydrate esterase

**GH:** Glycoside hydrolase

**ITS2**: Internal transcribed spacer region 2

**KO:** KEGG Ontology categories

**LC-MS/MS:** Liquid chromatography with tandem mass spectrometry

**ORF:** Open reading frame

**OTUs:** Operational taxonomic units

**PBS:** Phosphate buffered saline

**PCR:** Polymerase chain reaction

**PL:** Polysaccharide lyase

**TPM:** Transcripts per million

## Ethics approval and consent to participate

Not applicable

## Consent for publication

Not applicable

## Availability of data and material

Metaproteomic and metatranscriptomic databases generated during this research are available at MassIVE (https://massive.ucsd.edu/) MSV000083872 and ProteomeXchange

(http://www.proteomexchange.org/) PXD014068. The raw 16S rRNA gene sequencing data generated and analysed in this study is available from the European Nucleotide Archive (https://www.ebi.ac.uk/ena) under accessions PRJEB32810 and ERP115532. A curated dataset is available in the supplemental dataset found in Additional file 2. In-house scripts, datasets and dependencies for reproducing this analysis is available at https://github.com/leadbot/Salt-marsh-metasecretome-analysis.

## Competing interests

The authors declare no conflict of interest.


## Funding

This work was funded by Biotechnology and Biological Sciences Research Council (BBSRC) Grants BB/K020358/1, BB/I018492/1 and BB/L001926/1. D.R.L. and N.C.O. were supported by a studentship from the BBSRC Doctoral Training Programme (BB/J014443/1). J.SA. was supported by the Brazilian National Council for Scientific and Technology Development (CNPq; process number: 232506/2014-0).


## Authors' contributions

N.C.B. and S.J.M.-M. conceived the idea, provided expertise and edited the manuscript. D.R.L., N.C.B., S.J.M.-M. and T.H. designed experiments. D.R.L. conducted experiments and analyzed the data, wrote and edited the manuscript. Y.L. performed RNA-seq assembly. A.A.D. performed mass spectroscopy and assisted with the MS/MS analysis. N.C.O. and J.P.B., assisted in data handling,

protein expression and provided significant expertise and intellectual input. J.D.T. provided expertise and assisted in developing the phylogenetic analysis pipeline. J.S.A. provided intellectual input. A.S. assisted in cloning. A.M.A. assisted in method development.

**Acknowledgements**

The authors thank Dr. Deborah Rathbone and Susan Heywood at the Biorenewables Development Centre (York, UK) for access to research facilities and providing invaluable expertise and assistance. The York Centre of Excellence in Mass Spectrometry was created thanks to investment through Science City York, supported by Yorkshire Forward with funds from the Northern Way Initiative, and subsequent support from EPSRC (EP/K039660/1; EP/M028127/1).

**Authors' information**

Not applicable

**References**

1. Morris JT, Sundberg K, Hopkinson CS: Salt Marsh Primary Production and Its Responses to Relative Sea Level and Nutrients in Estuaries at Plum Island, Massachusetts, and North Inlet, South Carolina, USA. Oceanography. 2013;26:78-84.
2. Trilla GG, De Marco S, Marcovecchio J, Vicari R, Kandus P: Net Primary Productivity of *Spartina densiflora* Brong in an SW Atlantic Coastal Salt Marsh. Estuaries and Coasts. 2010;33:953-962.
3. Vera F, Gutierrez JL, Ribeiro PD: Aerial and detritus production of the cordgrass *Spartina densiflora* in a southwestern Atlantic salt marsh. Botany-Botanique. 2009;87:482-491.
4. Chmura GL: What do we need to assess the sustainability of the tidal salt marsh carbon sink? Ocean & Coastal Management. 2013;83:25-31.
5. Hopkinson CS, Cai WJ, Hu XP: Carbon sequestration in wetland dominated coastal systems - a global sink of rapidly diminishing magnitude. Current Opinion in Environmental Sustainability. 2012;4:186-194.
6. Ouyang X, Lee SY: Updated estimates of carbon accumulation rates in coastal marsh sediments. Biogeosciences. 2014;11:5057-5071.
7. McLeod E, Chmura GL, Bouillon S, Salm R, Bjork M, Duarte CM, Lovelock CE, Schlesinger WH, Silliman BR: A blueprint for blue carbon: toward an improved understanding of the role of vegetated coastal habitats in sequestering CO2. Frontiers in Ecology and the Environment. 2011; 9:552-560.

8. Chmura GL, Anisfeld SC, Cahoon DR, Lynch JC: Global carbon sequestration in tidal, saline wetland soils. Global Biogeochemical Cycles. 2003;17:12.
9. Bouchard V, Lefeuvre JC: Primary production and macro-detritus dynamics in a European salt marsh: carbon and nitrogen budgets. Aquatic Botany. 2000;67:23-42.
10. Fogel ML, Sprague EK, Gize AP, Frey RW: Diagenesis of organic-matter in georgia salt marshes. Estuarine Coastal and Shelf Science. 1989;28:211-230.
11. Benner R, Fogel ML, Sprague EK, Hodson RE: Depletion of C-13 in lignin and its implications for stable carbon isotope studies. Nature. 1987;329:708-710.
12. Barry SC, Bianchi TS, Shields MR, Hutchings JA, Jacoby CA, Frazer TK: Characterizing blue carbon stocks in *Thalassia testudinum* meadows subjected to different phosphorus supplies: A lignin biomarker approach. Limnology and Oceanography. 2018;63:2630-2646.
13.Young LY, Frazer AC: The fate of lignin and lignin-derived compounds in anaerobic environments. Geomicrobiology Journal. 1987;5:261-293.
14.Hernes PJ, Robinson AC, Aufdenkampe AK: Fractionation of lignin during leaching and sorption and implications for organic matter "freshness". Geophysical Research Letters. 2007;34:6.
15.Bianchi TS, Cui XQ, Blair NE, Burdige DJ, Eglinton TI, Galy V: Centers of organic carbon burial and oxidation at the land-ocean interface. Organic Geochemistry. 2018;115:138-155.
16. Hemingway JD, Rothman DH, Grant KE, Rosengard SZ, Eglinton TI, Derry LA, Galy VV: Mineral protection regulates long-term global preservation of natural organic carbon. Nature. 2019;570:228.
17. Macreadie PI, Allen K, Kelaher BP, Ralph PJ, Skilbeck CG: Paleoreconstruction of estuarine sediments reveal human-induced weakening of coastal carbon sinks. Global Change Biology. 2012;18:891-901.
18. Marriott PE, Gomez LD, McQueen-Mason SJ: Unlocking the potential of lignocellulosic biomass through plant science. New Phytologist. 2016;209:1366-1381.
19. Cragg SM, Beckham GT, Bruce NC, Bugg TDH, Distel DL, Dupree P, Etxabe AG, Goodell BS, Jellison J, McGeehan JE, et al: Lignocellulose degradation mechanisms across the Tree of Life. Current Opinion in Chemical Biology. 2015;29:108-119.
20. Jackson D, Long SP, Mason CF: Net primary production, decomposition and export of spartina-anglica on a suffolk salt-marsh. Journal of Ecology. 1986;74:647-662.
21. Dame RF, Stilwell D: Environmental-factors influencing macrodetritus flux in north inlet estuary. Estuarine Coastal and Shelf Science. 1984;18:721-726.
22. Buchan A, Newell SY, Butler M, Biers EJ, Hollibaugh JT, Moran MA: Dynamics of bacterial and fungal communities on decaying salt marsh grass. Applied and Environmental Microbiology. 2003;69:6676-6687.
23. Torzilli AP, Sikaroodi M, Chalkley D, Gillevet PM: A comparison of fungal communities from four salt marsh plants using automated ribosomal intergenic spacer analysis (ARISA). Mycologia. 2006;98:690-698.
24. Calado MD, Carvalho L, Barata M, Pang KL: Potential roles of marine fungi in the decomposition process of standing stems and leaves of *Spartina maritima*. Mycologia 2019, 111:371-383.
25. Torzilli AP, Andrykovitch G: Degradation of spartina lignocellulose by individual and mixed cultures of salt-marsh fungi. Canadian Journal of Botany-Revue Canadienne De Botanique. 1986;64:2211-2215.
26. Wilson JO, Buchsbaum R, Valiela I, Swain T: Decomposition in salt-marsh ecosystems - phenolic dynamics during decay of litter of S*partina alterniflora*. Marine Ecology Progress Series. 1986;29:177-187.
27. Baumann H, Wallace RB, Tagliaferri T, Gobler CJ: Large Natural pH, CO2 and O-2 Fluctuations in a Temperate Tidal Salt Marsh on Diel, Seasonal, and Interannual Time Scales. Estuaries and Coasts. 2015;38:220-231.

28. Negrin VL, Trilla GG, Kandus P, Marcovecchio JE: Decomposition and nutrient dynamics in a *Spartina alterniflora* marsh of the bahia blanca estuary, Argentina. Brazilian Journal of Oceanography. 2012;60:259-263.
29. White DA, Trapani JM, Thien LB, Weiss TE: Productivity and decomposition of dominant salt-marsh plants in Louisiana. Ecology. 1978;59:751-759.
30. Valiela I, Wilson J, Buchsbaum R, Rietsma C, Bryant D, Foreman K, Teal J: Importance of chemical-composition of salt-marsh litter on decay-rates and feeding by detritivores. Bulletin of Marine Science. 1984;35:261-269.
31. Bouchard V, Creach V, Lefeuvre JC, Bertru G, Mariotti A: Fate of plant detritus in a European salt marsh dominated by *Atriplex portulacoides* (L.) Aellen. Hydrobiologia. 1998;374:75-87.
32. Darjany LE, Whitcraft CR, Dillon JG: Lignocellulose-responsive bacteria in a southern California salt marsh identified by stable isotope probing. Frontiers in Microbiology. 2014;5:9.
33. Benner R, Newell SY, Maccubbin AE, Hodson RE: Relative contributions of bacteria and fungi to rates of degradation of lignocellulosic detritus in salt-marsh sediments. Applied and Environmental Microbiology. 1984;48:36-40.
34. Cortes-Tolalpa L, Norder J, van Elsas JD, Salles JF: Halotolerant microbial consortia able to degrade highly recalcitrant plant biomass substrate. Applied Microbiology and Biotechnology. 2018;102:2913-2927.
35. Alessi AM, Bird SM, Bennett JP, Oates NC, Li Y, Dowle AA, Polikarpov I, Young JPW, McQueen-Mason SJ, Bruce NC: Revealing the insoluble metasecretome of lignocellulose-degrading microbial communities. Scientific Reports. 2017;7.
36. Quast C, Pruesse E, Yilmaz P, Gerken J, Schweer T, Yarza P, Peplies J, Glockner FO: The SILVA ribosomal RNA gene database project: improved data processing and web-based tools. Nucleic Acids Research. 2013;41:D590-D596.
37. Langmead B, Salzberg SL: Fast gapped-read alignment with Bowtie 2. Nature Methods. 2012;9:357-U354.
38. Chen C, Khaleel SS, Huang H, Wu CH: Software for pre-processing Illumina next-generation sequencing short read sequences. Source code for biology and medicine. 2014;9:8.
39. Grabherr MG, Haas BJ, Yassour M, Levin JZ, Thompson DA, Amit I, Adiconis X, Fan L, Raychowdhury R, Zeng QD, et al: Full-length transcriptome assembly from RNA-Seq data without a reference genome. Nature Biotechnology. 2011;29:644-U130.
40. Perkins DN, Pappin DJC, Creasy DM, Cottrell JS: Probability-based protein identification by searching sequence databases using mass spectrometry data. Electrophoresis. 1999;20:3551-3567.
41. Ishihama Y, Oda Y, Tabata T, Sato T, Nagasu T, Rappsilber J, Mann M: Exponentially modified protein abundance index (emPAI) for estimation of absolute protein amount in proteomics by the number of sequenced peptides per protein. Molecular & Cellular Proteomics. 2005;4:1265-1272.
42. Yin YB, Mao XZ, Yang JC, Chen X, Mao FL, Xu Y: dbCAN: a web resource for automated carbohydrate-active enzyme annotation. Nucleic Acids Research. 2012;40:W445-W451.
43. Camacho C, Coulouris G, Avagyan V, Ma N, Papadopoulos J, Bealer K, Madden TL: BLAST plus : architecture and applications. Bmc Bioinformatics. 2009;10:9.
44. Huerta-Cepas J, Serra F, Bork P: ETE 3: Reconstruction, Analysis, and Visualization of Phylogenomic Data. Molecular Biology and Evolution. 2016;33:1635-1638.
45. Parada AE, Needham DM, Fuhrman JA: Every base matters: assessing small subunit rRNA primers for marine microbiomes with mock communities, time series and global field samples. Environmental Microbiology. 2016;18:1403-1414.
46. Apprill A, McNally S, Parsons R, Weber L: Minor revision to V4 region SSU rRNA 806R gene primer greatly increases detection of SAR11 bacterioplankton. Aquatic Microbial Ecology. 2015;75:129-137.
47. Ihrmark K, Bodeker ITM, Cruz-Martinez K, Friberg H, Kubartova A, Schenck J, Strid Y, Stenlid J, Brandstrom-Durling M, Clemmensen KE, Lindahl BD: New primers to amplify the fungal ITS2

region - evaluation by 454-sequencing of artificial and natural communities. Fems Microbiology. Ecology 2012;82:666-677.
48. Tedersoo L, Bahram M, Polme S, Koljalg U, Yorou NS, Wijesundera R, Ruiz LV, Vasco-Palacios AM, Thu PQ, Suija A, et al: Global diversity and geography of soil fungi. Science. 2014;346:1078.
49. Lundberg DS, Yourstone S, Mieczkowski P, Jones CD, Dangl JL: Practical innovations for high-throughput amplicon sequencing. Nature Methods. 2013;10:999.
50. Rognes T, Flouri T, Nichols B, Quince C, Mahe F: VSEARCH: a versatile open source tool for metagenomics. Peerj. 2016;4:22.
51. Bengtsson-Palme J, Ryberg M, Hartmann M, Branco S, Wang Z, Godhe A, De Wit P, Sanchez-Garcia M, Ebersberger I, de Sousa F, et al: Improved software detection and extraction of ITS1 and ITS2 from ribosomal ITS sequences of fungi and other eukaryotes for analysis of environmental sequencing data. Methods in Ecology and Evolution. 2013;4:914-919.
52. Edgar RC: Search and clustering orders of magnitude faster than BLAST. Bioinformatics. 2010;26:2460-2461.
53. Edgar RC: UPARSE: highly accurate OTU sequences from microbial amplicon reads. Nature Methods. 2013;10:996.
54. Caporaso JG, Kuczynski J, Stombaugh J, Bittinger K, Bushman FD, Costello EK, Fierer N, Pena AG, Goodrich JK, Gordon JI, et al: QIIME allows analysis of high-throughput community sequencing data. Nature Methods. 2010;7:335-336.
55. Koljalg U, Nilsson RH, Abarenkov K, Tedersoo L, Taylor AFS, Bahram M, Bates ST, Bruns TD, Bengtsson-Palme J, Callaghan TM, et al: Towards a unified paradigm for sequence-based identification of fungi. Molecular Ecology. 2013;22:5271-5277.
56. Nguyen NH, Song ZW, Bates ST, Branco S, Tedersoo L, Menke J, Schilling JS, Kennedy PG: FUNGuild: An open annotation tool for parsing fungal community datasets by ecological guild. Fungal Ecology. 2016;20**:**241-248.
57. Hagberg A, Swart P, S Chult D: Exploring network structure, dynamics, and function using NetworkX. Proceedings of the 7th Python in Science conference. 2008;11-15.
58. Marriott PE, Sibout R, Lapierre C, Fangel JU, Willats WGT, Hofte H, Gomez LD, McQueen-Mason SJ: Range of cell-wall alterations enhance saccharification in *Brachypodium distachyon* mutants. Proceedings of the National Academy of Sciences of the United States of America. 2014;111:14601-14606.
59. Updegraff DM: Semimicro determination of cellulose in biological materials. Analytical Biochemistry. 1969;32:420.
60. Saeman JF: Kinetics of wood saccharification - hydrolysis of cellulose and decomposition of sugars in dilute acid at high temperature. Industrial and Engineering Chemistry. 1945;37:43-52.
61. Moreira-Vilar FC, Siqueira-Soares RD, Finger-Teixeira A, de Oliveira DM, Ferro AP, da Rocha GJ, Ferrarese MDL, dos Santos WD, Ferrarese O: The Acetyl Bromide Method Is Faster, Simpler and Presents Best Recovery of Lignin in Different Herbaceous Tissues than Klason and Thioglycolic Acid Methods. Plos One. 2014;9:7.
62. Foster CE, Martin TM, Pauly M: Comprehensive compositional analysis of plant cell walls (lignocellulosic biomass) part I: lignin. Journal of visualized experiments: JoVE. 2010.
63. Jones E, Oliphant T, Peterson P: SciPy: Open source scientific tools for Python. 2001.
64. Pedregosa F, Varoquaux G, Gramfort A, Michel V, Thirion B, Grisel O, Blondel M, Prettenhofer P, Weiss R, Dubourg VJJomlr: Scikit-learn: Machine learning in Python. 2011;12:2825-2830.
65. Alessi AM, Bird SM, Oates NC, Li Y, Dowle AA, Novotny EH, deAzevedo ER, Bennett JP, Polikarpov I, Young JPW, et al: Defining functional diversity for lignocellulose degradation in a microbial community using multi-omics studies. Biotechnology for Biofuels. 2018;11:16.
66. Valiela I, Teal JM, Allen SD, Vanetten R, Goehringer D, Volkmann S: Decomposition in salt-marsh ecosystems - the phases and major factors affecting disappearance of above-ground organic-matter. Journal of Experimental Marine Biology and Ecology. 1985; 89:29-54.

67. Curco A, Ibanez C, Day JW, Prat N: Net primary production and decomposition of salt marshes of the Ebre delta (Catalonia, Spain). Estuaries. 2002;25:309-324.
68. Simoes MP, Calado ML, Madeira M, Gazarini LC: Decomposition and nutrient release in halophytes of a Mediterranean salt marsh. Aquatic Botany. 2011;94:119-126.
69. Cragg SM, Friess DA, Gillis LG, Trevathan-Tackett SM, Terrett OM, Watts JEM, Distel DL, Dupree P: Vascular Plants Are Globally Significant Contributors to Marine Carbon Fluxes and Sinks. In Annual Review of Marine Science. 2020;12:469-497: Annual Review of Marine Science.
70. Benner R, Fogel ML, Sprague EK: Diagenesis of belowground biomass of *Spartina alterniflora* in salt-marsh sediments. Limnology and Oceanography. 1991;36:1358-1374.
71. Wilson JO, Valiela I, Swain T: Carbohydrate dynamics during decay of litter of *Spartina alterniflora*. Marine Biology. 1986;92:277-284.
72. Maccubbin AE, Hodson RE: Mineralization of detrital lignocelluloses by salt-marsh sediment microflora. Applied and Environmental Microbiology. 1980;40:735-740.
73. Nakamura AM, Nascimento AS, Polikarpov I: Structural diversity of carbohydrate esterases. Biotechnology Research and Innovation. 2017;1:35-51.
74. Buanafina MMD: Feruloylation in Grasses: Current and Future Perspectives. Molecular Plant. 2009;2:861-872.
75. Chiniquy D, Sharma V, Schultink A, Baidoo EE, Rautengarten C, Cheng K, Carroll A, Ulvskov P, Harholt J, Keasling JD, et al: XAX1 from glycosyltransferase family 61 mediates xylosyltransfer to rice xylan. Proceedings of the National Academy of Sciences of the United States of America. 2012;109:17117-17122.
76. de Souza WR, Martins PK, Freeman J, Pellny TK, Michaelson LV, Sampaio BL, Vinecky F, Ribeiro AP, da Cunha B, Kobayashi AK, et al: Suppression of a single BAHD gene in Setaria viridis causes large, stable decreases in cell wall feruloylation and increases biomass digestibility. New Phytologist. 2018;218:81-93.
77. Grantham NJ, Wurman-Rodrich J, Terrett OM, Lyczakowski JJ, Stott K, Iuga D, Simmons TJ, Durand-Tardif M, Brown SP, Dupree R, et al: An even pattern of xylan substitution is critical for interaction with cellulose in plant cell walls. Nature Plants. 2017;3:859-865.
78. Haddad RI, Newell SY, Martens CS, Fallon RD: Early diagenesis of lignin-associated phenolics in the salt-marsh grass *Spartina alterniflora*. Geochimica Et Cosmochimica Acta. 1992;56:3751-3764.
79. Alzarhani AK, Clark DR, Underwood GJC, Ford H, Cotton TEA, Dumbrell AJ: Are drivers of root-associated fungal community structure context specific? Isme Journal. 2019;13**:**1330-1344.
80. Wilhelm RC, Singh R, Eltis LD, Mohn WW: Bacterial contributions to delignification and lignocellulose degradation in forest soils with metagenomic and quantitative stable isotope probing. Isme Journal. 2019;13:413-429.
81. Lee SH, Megonigal PJ, Langley AJ, Kang H: Elevated CO2 and nitrogen addition affect the microbial abundance but not the community structure in salt marsh ecosystem. Applied Soil Ecology. 2017;117:129-136.
82. Chaudhary DR, Kim J, Kang H: Influences of Different Halophyte Vegetation on Soil Microbial Community at Temperate Salt Marsh. Microbial Ecology. 2018;75:729-738.
83. Cleary DFR, Coelho F, Oliveira V, Gomes NCM, Polonia ARM: Sediment depth and habitat as predictors of the diversity and composition of sediment bacterial communities in an inter-tidal estuarine environment. Marine Ecology-an Evolutionary Perspective. 2017;38:15.
84. Taylor LE, Henrissat B, Coutinho PM, Ekborg NA, Hutcheson SW, Weiner RA: Complete cellulase system in the marine bacterium *Saccharophagus degradans* strain 2-40(T). Journal of Bacteriology. 2006;188:3849-3861.
85. Ekborg NA, Gonzalez JM, Howard MB, Taylor LE, Hutcheson SW, Weiner RM: *Saccharophagus degradans* gen. nov., sp nov., a versatile marine degrader of complex polysaccharides. International Journal of Systematic and Evolutionary Microbiology. 2005;55:1545-1549.

86. Jung YH, Kim HK, Song DS, Choi IG, Yang TH, Lee HJ, Seung D, Kim KH: Feasibility test of utilizing Saccharophagus degradans 2-40(T) as the source of crude enzyme for the saccharification of lignocellulose. Bioprocess and Biosystems Engineering. 2014;37:707-710.
87. Zhang HT, Hutcheson SW: Complex Expression of the Cellulolytic Transcriptome of *Saccharophagus degradans*. Applied and Environmental Microbiology. 2011;77:5591-5596.
88. Weiner RM, Taylor LE, Henrissat B, Hauser L, Land M, Coutinho PM, Rancurel C, Saunders EH, Longmire AG, Zhang HT, et al: Complete genome sequence of the complex carbohydrate-degrading marine bacterium, *Saccharophagus degradans* strain 2-40(T). Plos Genetics. 2008;4:13.
89. Fowler CA, Hemsworth GR, Cuskin F, Hart S, Turkenburg J, Gilbert HJ, Walton PH, Davies GJ: Structure and function of a glycoside hydrolase family 8 endoxylanase from *Teredinibacter turnerae*. Acta Crystallographica Section D-Structural Biology. 2018;74:946-955.
90. Fowler CA, Sabbadin F, Ciano L, Hemsworth GR, Elias L, Bruce N, McQueen-Mason S, Davies GJ, Walton PH: Discovery, activity and characterisation of an AA10 lytic polysaccharide oxygenase from the shipworm symbiont *Teredinibacter turnerae*. Biotechnology for Biofuels. 2019;12:11.
91. Yang JC, Madupu R, Durkin AS, Ekborg NA, Pedamallu CS, Hostetler JB, Radune D, Toms BS, Henrissat B, Coutinho PM, et al: The Complete Genome of *Teredinibacter turnerae* T7901: An Intracellular Endosymbiont of Marine Wood-Boring Bivalves (Shipworms). Plos One. 2009;4:17.
92. Ekborg NA, Morrill W, Burgoyne AM, Li L, Distell DL: CelAB, a multifunctional cellulase encoded by *Teredinibacter turnerae* T7902(T), a culturable symbiont isolated from the wood-boring marine bivalve Lyrodus pedicellatus. Applied and Environmental Microbiology. 2007;73:7785-7788.
93. Distel DL, Morrill W, MacLaren-Toussaint N, Franks D, Waterbury J: Teredinibacter turnerae gen. nov., sp nov., a dinitrogen-fixing, cellulolytic, endosymbiotic gamma-proteobacterium isolated from the gills of wood-boring molluscs (Bivalvia : *Teredinidae*). International Journal of Systematic and Evolutionary Microbiology. 2002;52:2261-2269.
94. Varnai A, Siika-aho M, Viikari L: Carbohydrate-binding modules (CBMs) revisited: reduced amount of water counterbalances the need for CBMs. Biotechnology for Biofuels. 2013;6:11.
95. Bowen JL, Morrison HG, Hobbie JE, Sogin ML: Salt marsh sediment diversity: a test of the variability of the rare biosphere among environmental replicates. Isme Journal. 2012;6:2014-2023.
96. Andrews JE, Samways G, Dennis PF, Maher BA: Origin, abundance and storage of organic carbon and sulphur in the Holocene Humber Estuary: emphasizing human impact on storage changes. Geological Society, London, Special Publications. 2000;166:145.
97. Lamb AL, Vane CH, Wilson GP, Rees JG, Moss-Hayes VL: Assessing delta C-13 and C/N ratios from organic material in archived cores as Holocene sea level and palaeoenvironmental indicators in the Humber Estuary, UK. Marine Geology. 2007;244:109-128.
98. Sechovcova H, Kulhava L, Fliegerova K, Trundova M, Morais D, Mrazek J, Kopecny J: Comparison of enzymatic activities and proteomic profiles of Butyrivibrio fibrisolvens grown on different carbon sources. Proteome Science. 2019;17:12.
99. Hunter JD: Matplotlib: A 2D graphics environment. Computing in Science & Engineering. 2007;9:90-95.

997

998

999 **Figure 1.** Schematic representation of the integrated 'omics approach undertaken in this study.

1000

1001 **Figure 2.** Temporal changes in lignocellulose composition and the distribution of carbohydrate active
1002 enzyme domains within the meta-exo-proteome. **a;** Lignocellulose composition of remaining *in situ*
1003 *Spartina anglica* biomass. **b;** Rate of compositional change within the lignocellulose displayed as
1004 µg.mg biomass$^{-1}$, the dashed line represents 0 change, *L*: Lignin, *H*: Hemicellulose, *C:* Cellulose. **c;**
1005 Euclidean clustering of the enzyme class profile (≤ 1e$^{-10}$), the 30 most abundant classes are displayed,
1006 *GH:* Glycoside hydrolase, *CE:* Carbohydrate esterase, *AA:* Auxiliary activity, *PL:* Polysaccharide lyase.
1007 **d;** Euclidean clustering of the carbohydrate binding domain (CBM) profile (≤ 1e$^{-10}$). Error bars (**a**)
1008 represent SE (n=25). Figure plotted with [99].

1009

1010 **Figure 3**. CAZyme producing taxa at family level resolution and their respective CAZyme
1011 contributions. Microbiome and proteomic data is displayed as the mean of n=5 and n=3 respectively.
1012 **a;** Distribution of CAZyme producing lineages with respective CAZyme productivity (≤ 1e$^{-10}$), taxa
1013 below the dashed line were not identified in the community profile. **b;** bacteria profiles elucidated
1014 from 16S rRNA gene sequence homology, each time point is the mean of five biological replicates. **c;**
1015 CAZyme productive bacteria profile, the non-CAZyme productive taxa have been filtered, boxes
1016 display OTU richness, no further filtering was undertaken for these data. *NA:* Not assigned, *†:*
1017 CAZyme producer. Figure plotted with [99].

1018

1019 **Figure 4.** Network associations among meta-exo-proteome CAZyme classes and taxonomic lineages.
1020 Data displayed is the mean of the four time points. Node area is proportional to productivity and

abundance for taxa and CAZyme class respectively. Edge color and width is relative to output size. Taxa < 0.025 $\sum \bar{x}$ mol% with ≤ 5 edges and CAZyme classes < $1.25 \times 10^{-3} \sum \bar{x}$ mol% have been filtered. Glycoside hydrolases (GH) families; blue nodes, carbohydrate esterases (CE) families; red nodes, auxiliary activities (AA) families; orange nodes, polysaccharide lyases (PL) families; yellow nodes, carbohydrate binding domains (CBM) families; purple nodes. *NA:* Not assigned.

Supplementary Information for:

# Mechanistic strategies of microbial communities regulating lignocellulose deconstruction in a UK salt marsh

**Authors**

Daniel R. Leadbeater[1§], Nicola C. Oates[1], Joseph P. Bennett[1], Yi Li[1], Adam A. Dowle[2], Joe D. Taylor[4], Juliana Sanchez Alponti[1], Alexander T. Setchfield[1], Anna M. Alessi[1], Thorunn Helgason[3], Simon J. McQueen-Mason[1§], Neil C. Bruce[1§]

[1] Centre for Novel Agricultural Products, Department of Biology, University of York, York, YO10 5DD, UK.

[2] Bioscience Technology Facility, Department of Biology, University of York, York, YO10 5DD, UK.

[3] Department of Biology, University of York, York, YO10 5DD, UK.

[4] School of Chemistry and Biosciences, University of Bradford, Bradford, West Yorkshire, BD7 1DP, UK.

[§] Corresponding authors: N.C.B. (email: neil.bruce@york.ac.uk), S.J.M.-M. (email: simon.mcqueenmason@york.ac.uk) or D.R.L. (email: daniel.leadbeater@york.ac.uk).

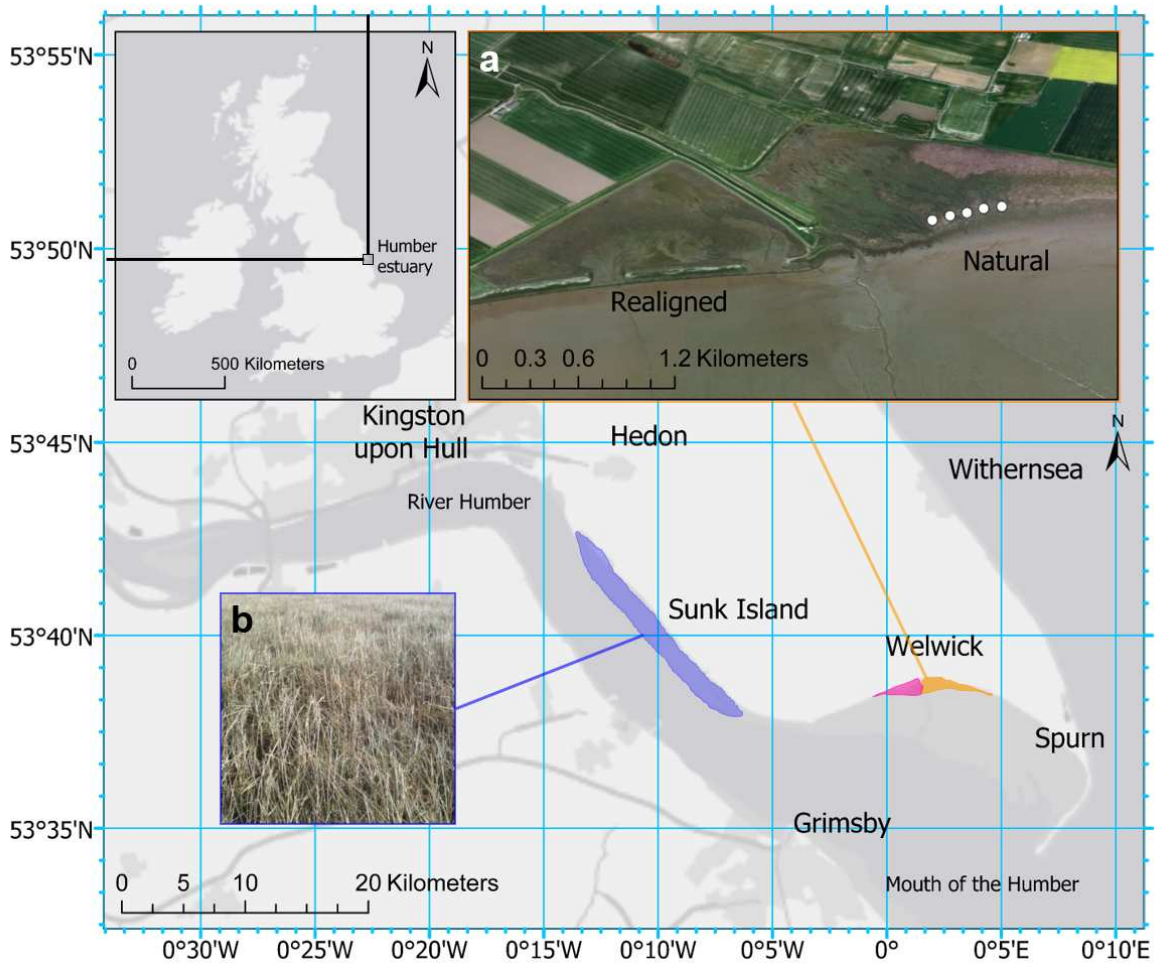


**Figure S1.** Experiment location. The Humber estuary (Hull, UK). The North bank of the Humber estuary, Welwick salt marsh (inlet a) is highlighted in orange and the cage locations along the transect in white within the inlet. Cherry Cobb Sands is highlighted in blue with the location of the collected Spartina anglica (inlet b).

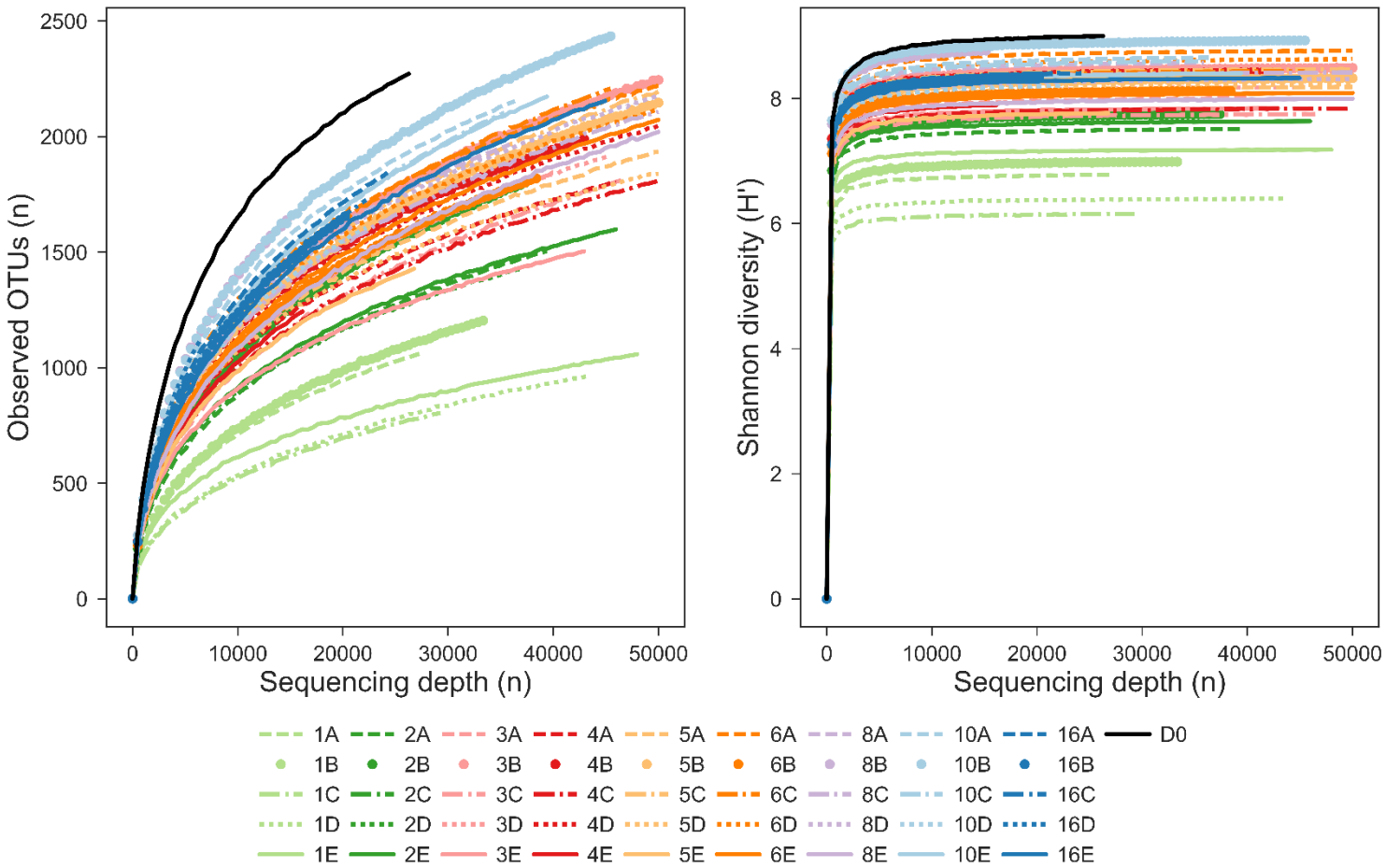


**Figure S2.** Coverage estimates for each 16S rRNA amplicon library for all biological replicates across each time point. **a;** Rarefaction curves identified by number of observed operational taxonomic units (OTUs) and sequencing depth. **b;** Shannon diversity index collector curves as a function of sequencing depth.

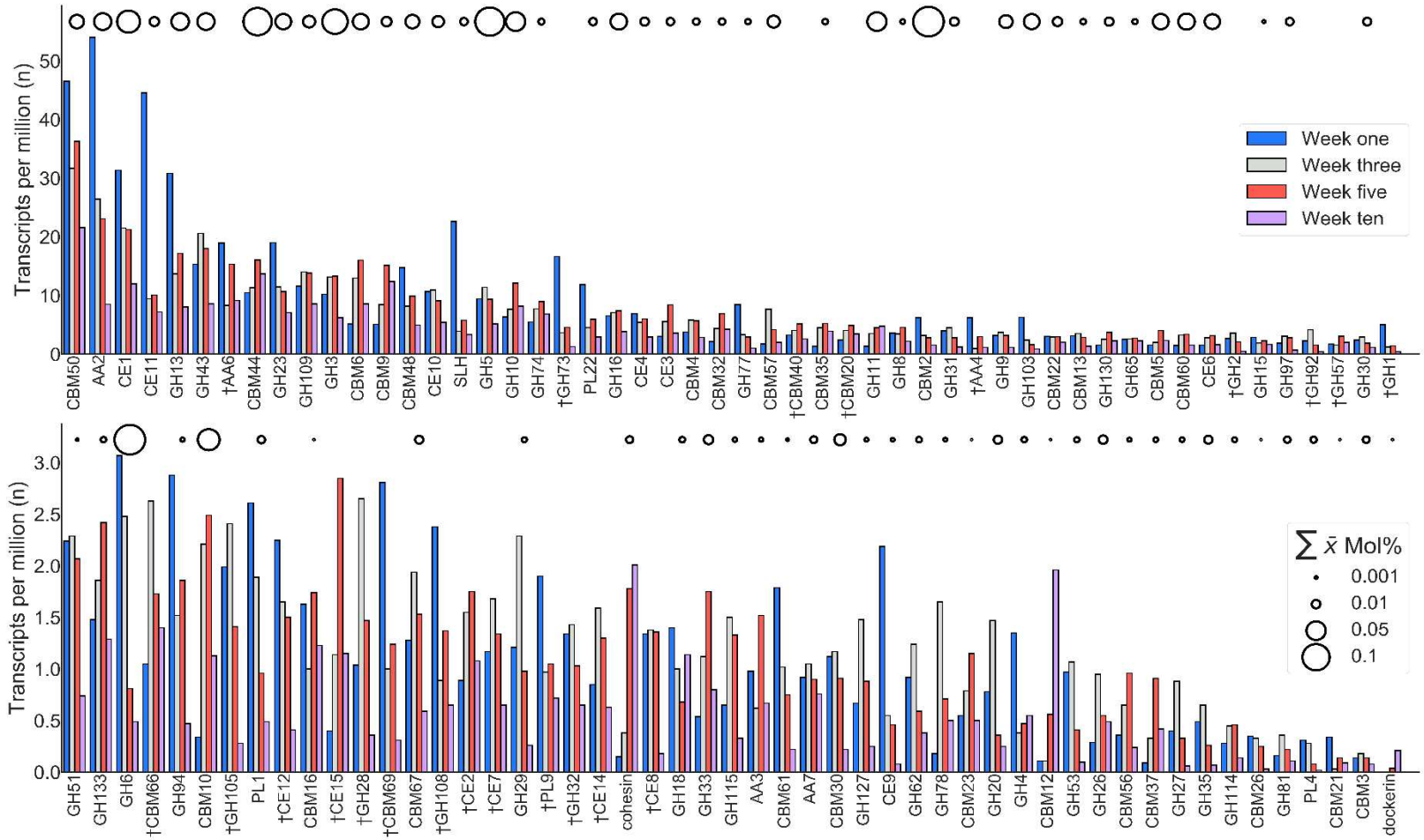


**Figure S3.** CAZyme families identified within the metatranscriptomic databases presented as transcripts per million (TPM). Glycosyl transferase families have been filtered and only annotations with expect values ≤ $1e^{-5}$ and TPM values ≥ 1 have been included for analysis. **†** delineates the CAZyme family was not identified within the meta-exo-proteome. Marker size is proportional to the mean sum of the molar percentage across the exo-meta-proteome for each week. *GH:* Glycoside hydrolase, *CE:* Carbohydrate esterase, *AA:* Auxiliary activity, *PL:* Polysaccharide lyase, *CBM:* Carbohydrate binding domain. Transcriptomic data includes both intracellular and extracellular representatives of the respective CAZyme families.

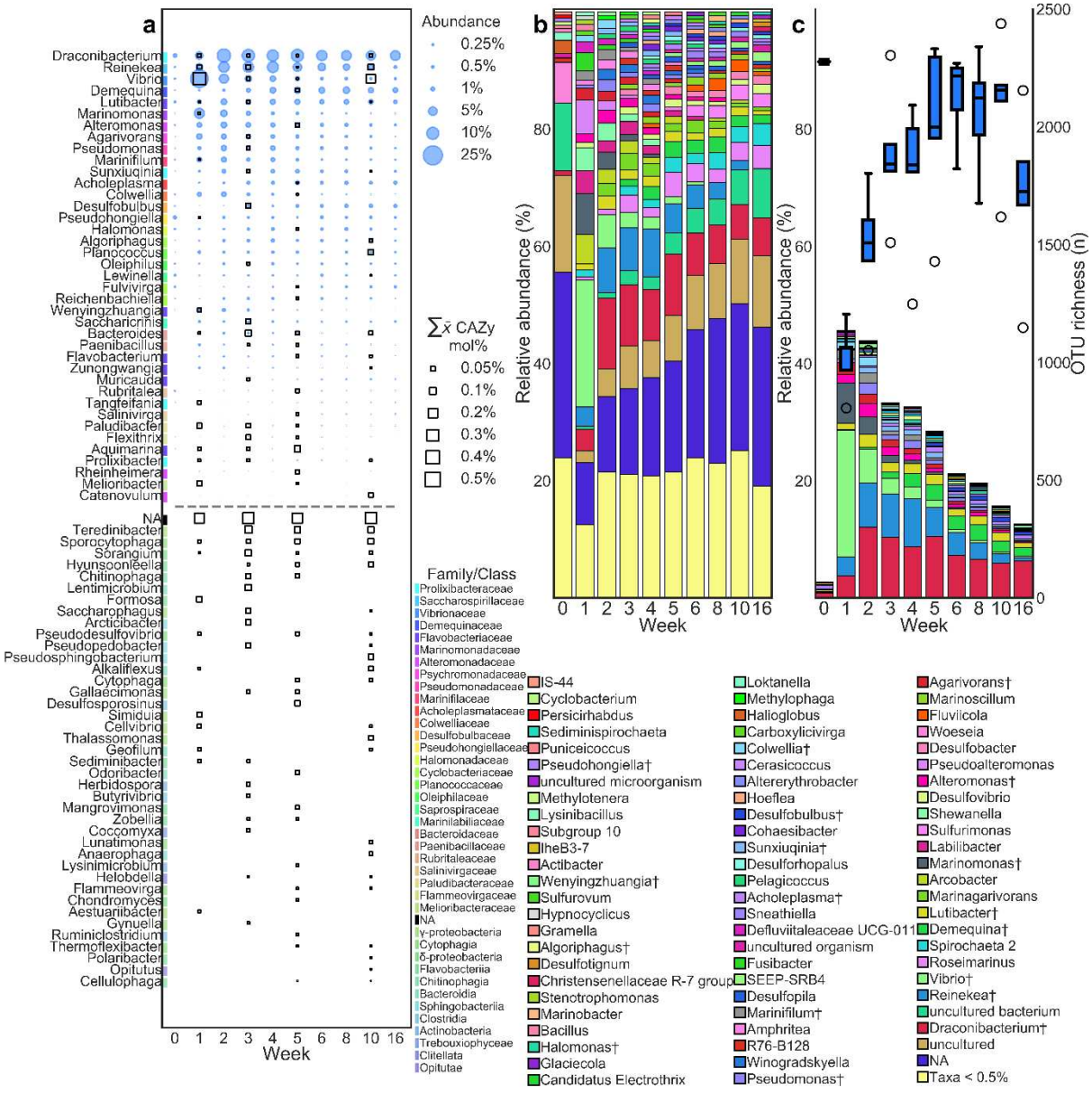


**Figure S4.** CAZyme producing genera and their respective CAZyme contributions. Microbiome and proteomic data is displayed as the mean of n=5 and n=3 respectively. **a;** Distribution of CAZyme producing lineages with respective CAZyme productivity (≤ $1e^{-10}$), taxa below the dashed line were not identified in the community profile, ordered by descending abundance by total temporal sum. **b;** Bacteria profiles elucidated from 16S rRNA sequence homology, each time point is the mean of five biological replicates. **c;** CAZyme productive bacteria profile, the non-CAZyme productive taxa have been filtered, boxes display OTU richness, no further filtering was undertaken for these data. *NA:* Not assigned, *†:* CAZyme producer.

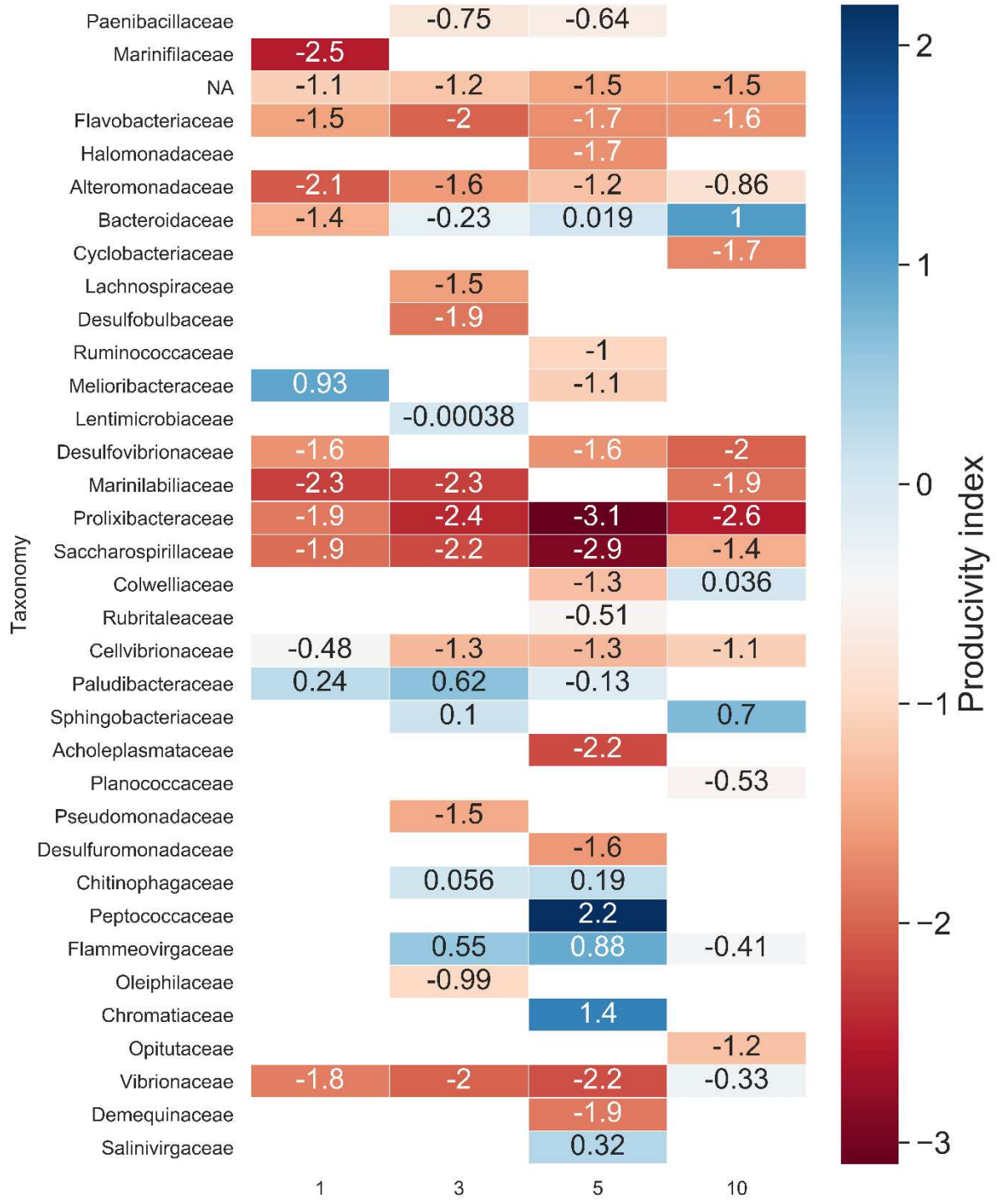


**Figure S5.** Productivity index for CAZyme producing taxa at family level resolution. A higher index indicates disproportionately more CAZyme produced per unit abundance. Values displayed as $\log_{10}(\sum \bar{x}$ mol%/Relative abundance).

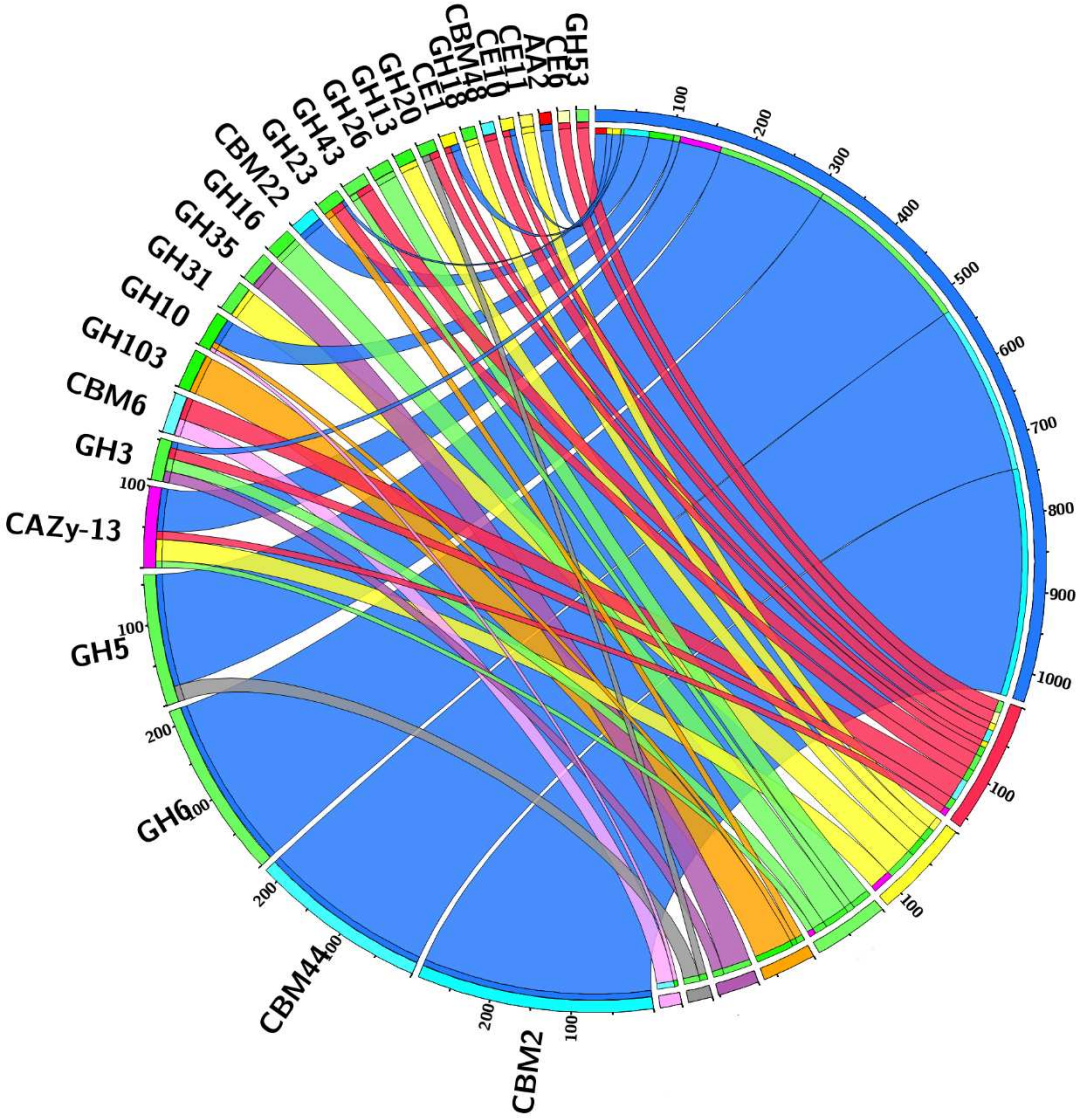


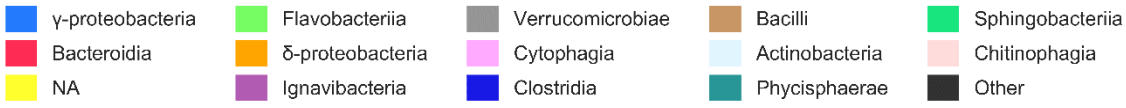


**Figure S6.** Phylogenetic distribution of CAZyme classes at class resolution for week one. Absolute values of segments are the sum molar percentage $1e^3$ (1000 = 1%). Ribbon size is relative to the contribution to or of the taxa/ CAZyme and are only interspecifically comparable. Taxa producing < 1% of the total CAZyme and CAZyme classes < 0.85% of the total have been filtered, no further proteomic filtering criteria was applied to this data. Chord diagrams were generated using the Circos software package [1]. *NA:* Not assigned.

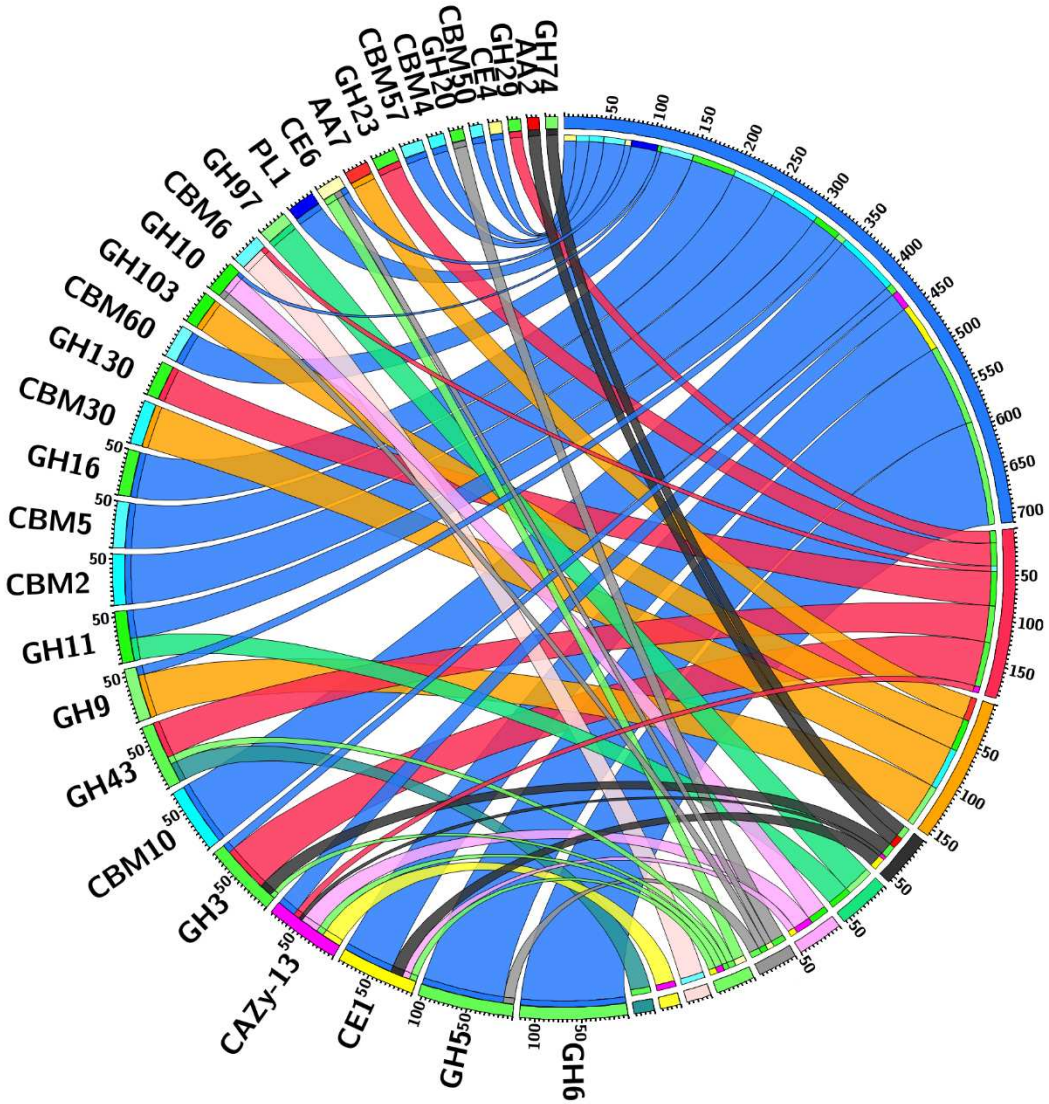


**Figure S7.** Phylogenetic distribution of CAZyme classes at class resolution for week three. Absolute values of segments are the sum molar percentage $1e^3$ (1000 = 1%). Ribbon size is relative to the contribution to or of the taxa/ CAZyme and are only interspecifically comparable. Taxa producing < 1% of the total CAZyme and CAZyme classes < 0.85% of the total have been filtered, no further proteomic filtering criteria was applied to this data. Chord diagrams were generated using the Circos software package [1]. *NA:* Not assigned.

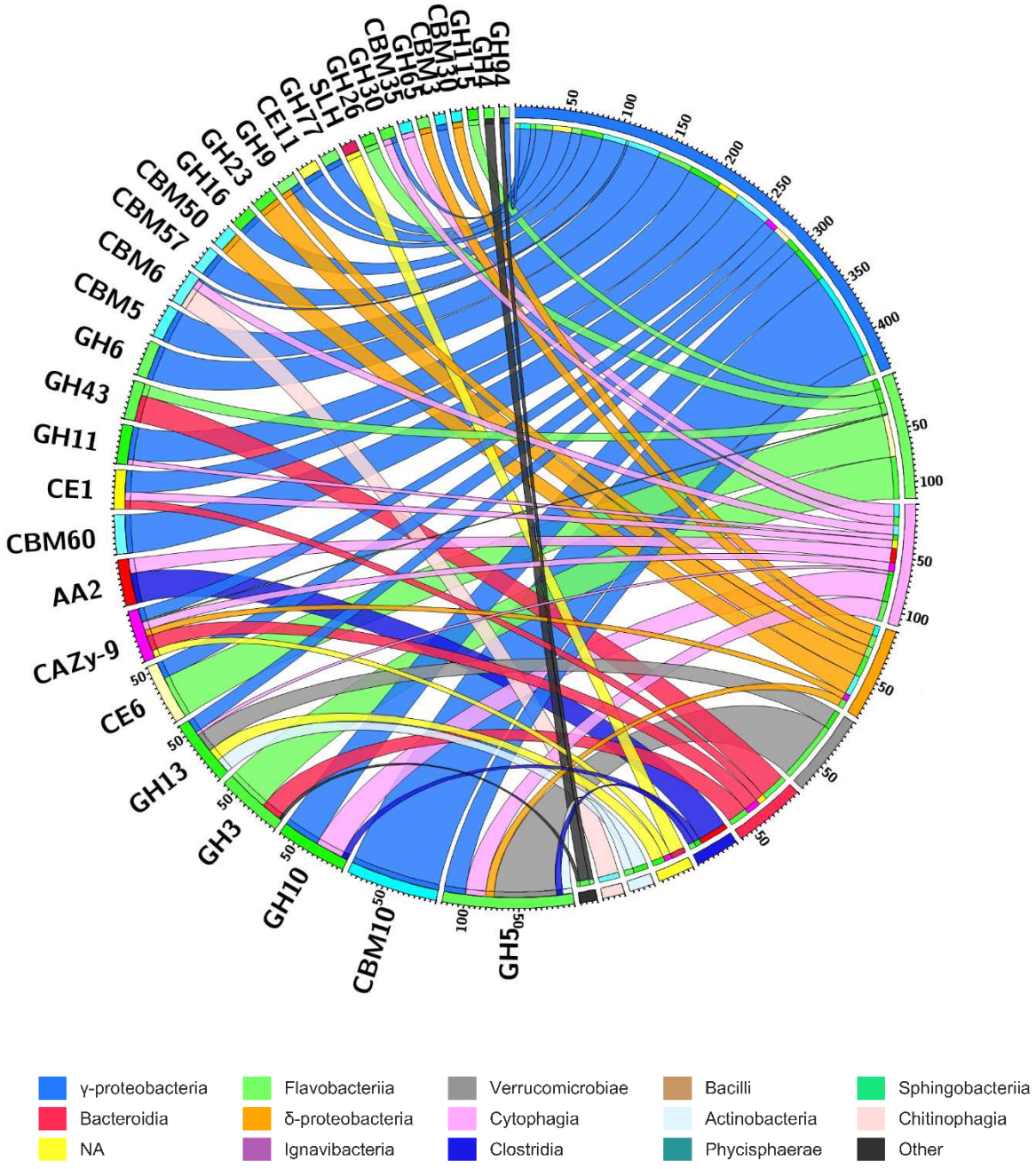


**Figure S8.** Phylogenetic distribution of CAZyme classes at class resolution for week five. Absolute values of segments are the sum molar percentage $1e^3$ (1000 = 1%). Ribbon size is relative to the contribution to or of the taxa/ CAZyme and are only interspecifically comparable. Taxa producing < 1% of the total CAZyme and CAZyme classes < 0.85% of the total have been filtered, no further proteomic filtering criteria was applied to this data. Chord diagrams were generated using the Circos software package [1]. *NA:* Not assigned.

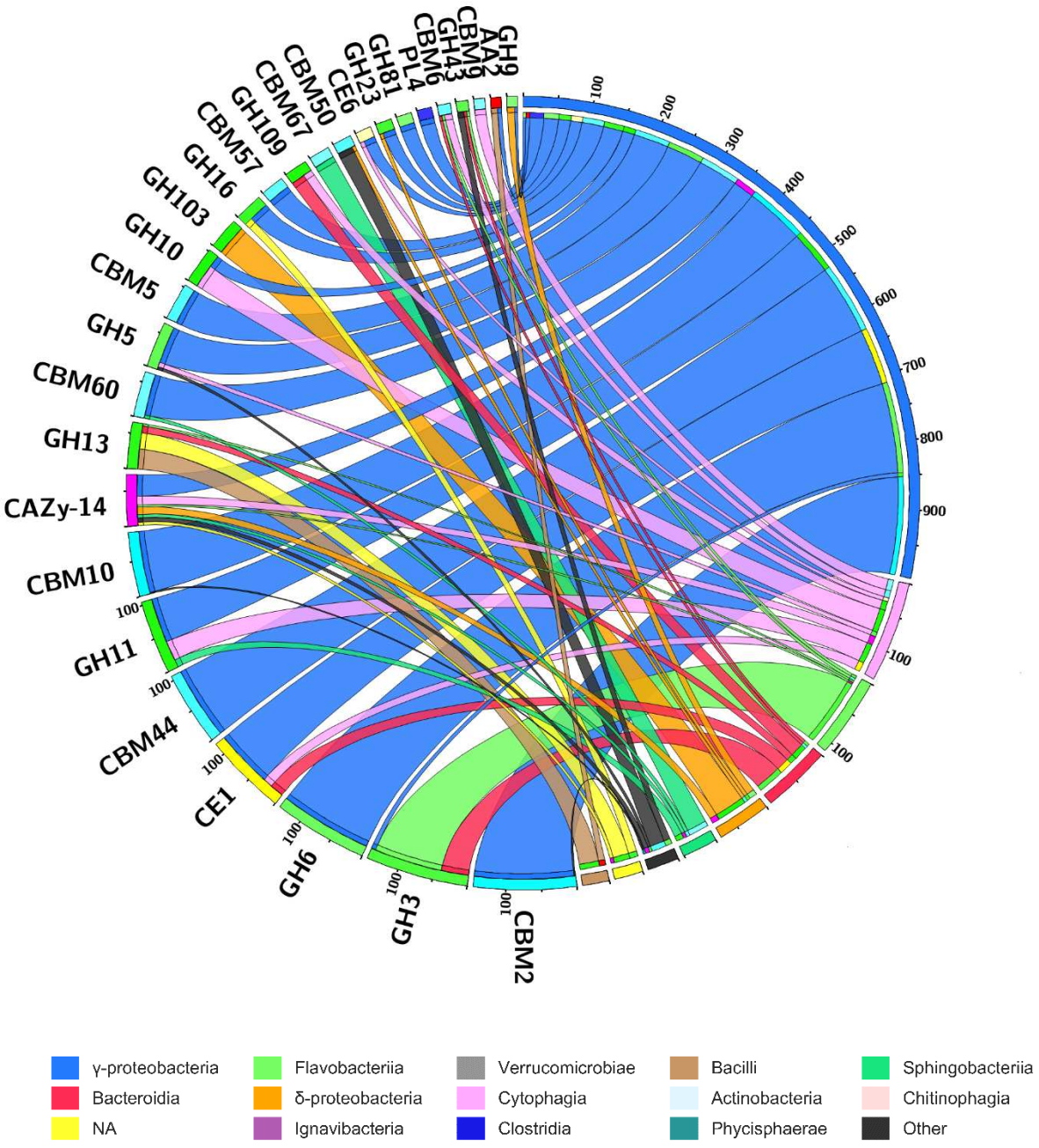


**Figure S9.** Phylogenetic distribution of CAZyme classes at class resolution for week ten. Absolute values of segments are the sum molar percentage $1e^3$ (1000 = 1%). Ribbon size is relative to the contribution to or of the taxa/ CAZyme and are only interspecifically comparable. Taxa producing < 1% of the total CAZyme and CAZyme classes < 0.85% of the total have been filtered, no further proteomic filtering criteria was applied to this data. Chord diagrams were generated using the Circos software package [1]. *NA:* Not assigned.

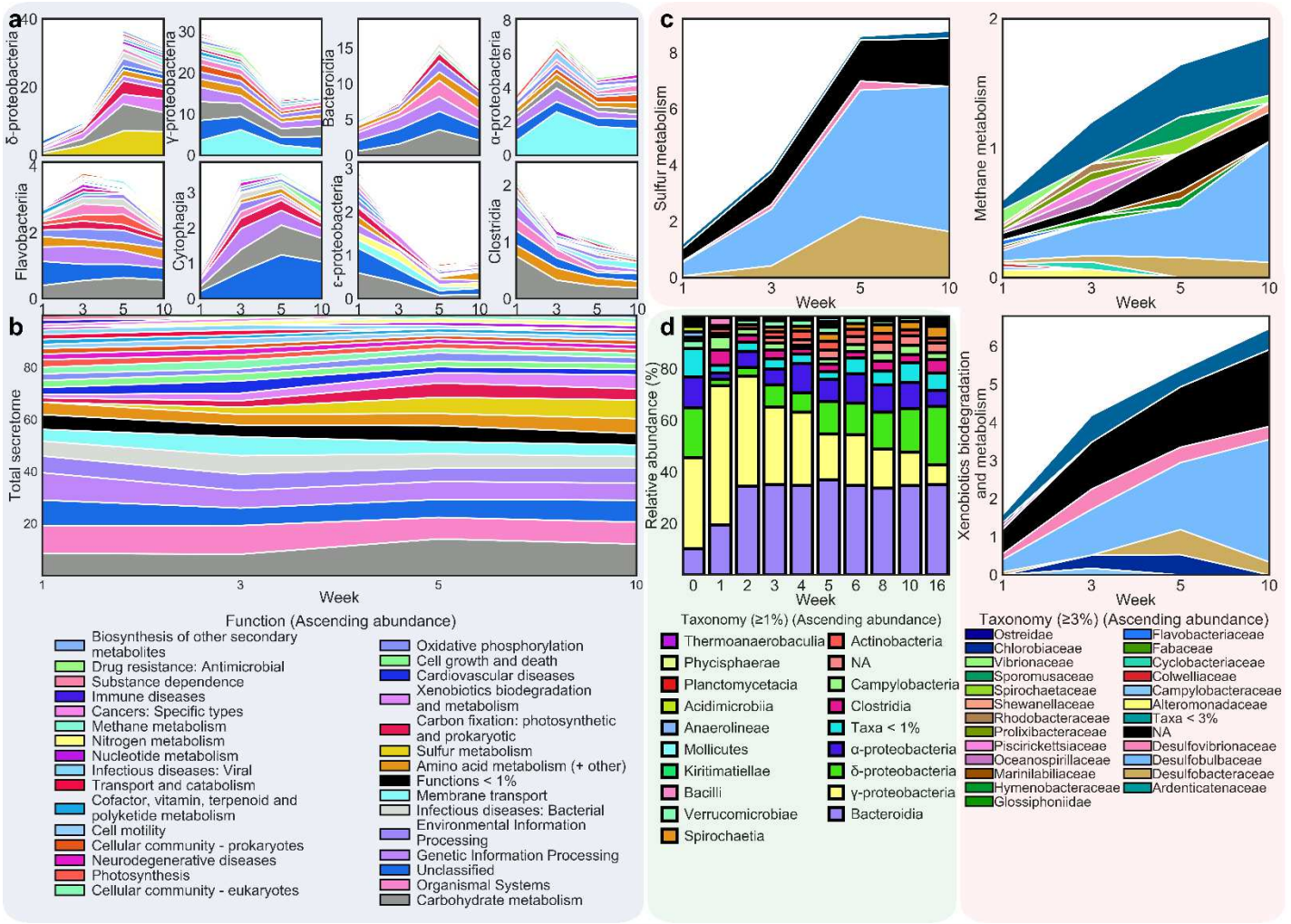


**Figure S10.** Functional classification of proteins within the metasecretome. Unclassified orthologs are not displayed. One to many mapping applied. **a;** Temporal distribution of functional KEGG orthologs [2] attributable to taxonomic classes (∑ x̄ mol%.) **b;** Functional assignment of the total metasecretome (∑ x̄ mol%). **c;** Taxonomic distribution of major functional pathways identified from the metasecretome (∑x̄ mol%). **d;** Bacteria profile. *NA:* Not assigned.

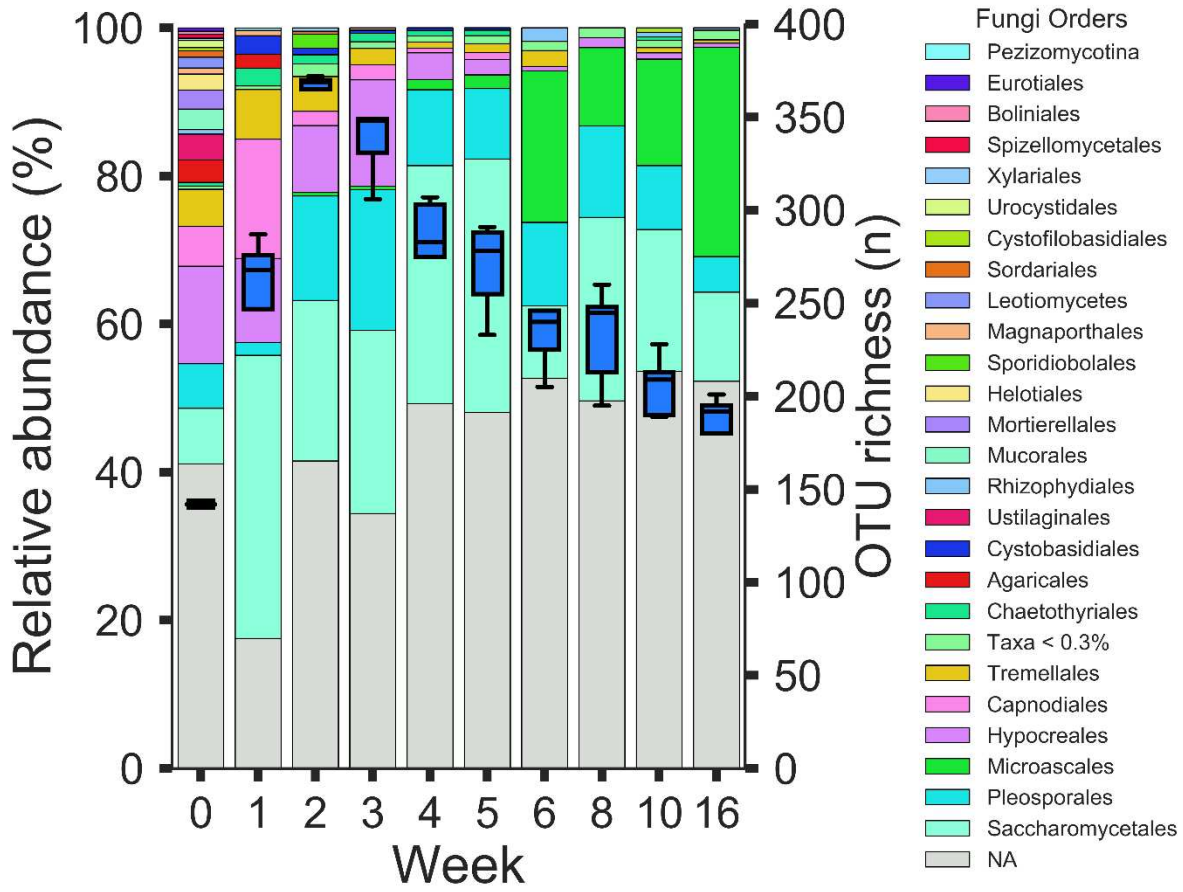


**Figure S11.** Fungal profiles and OTU richness elucidated from internal transcribed spacer region 2 amplicon sequencing across the 16-week time course. Data is displayed as the mean of n=5.

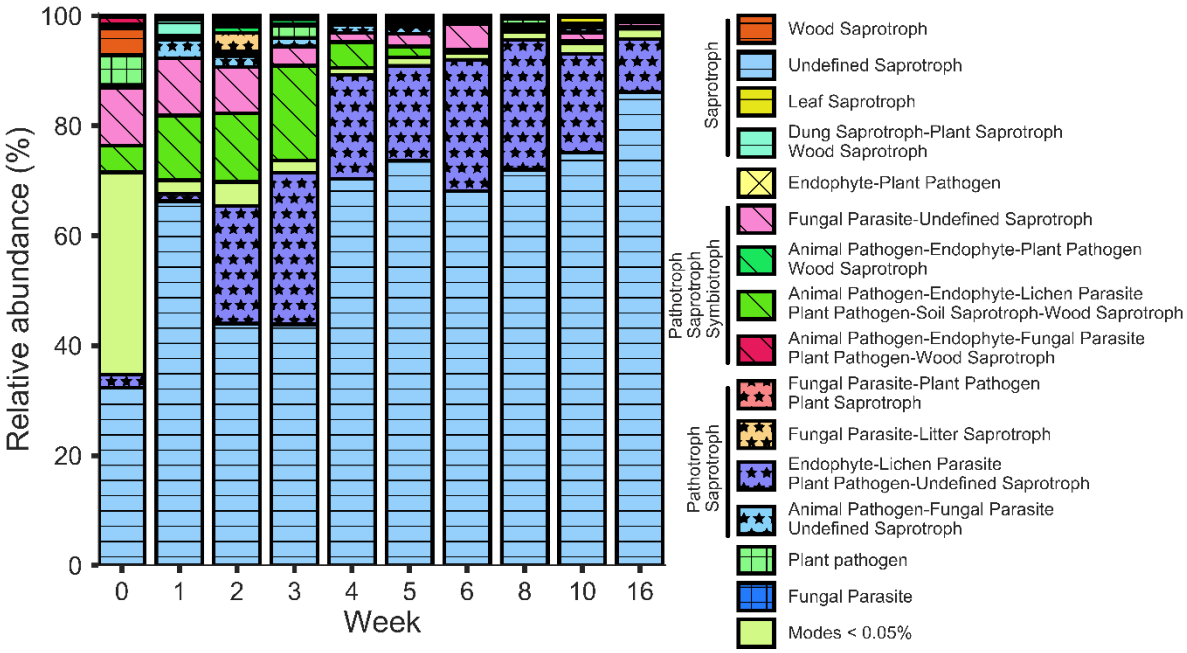


**Figure S12.** Nutrient acquisition strategy of fungi profile across the 16-week time course. Data is displayed as the mean of n=5. Guild and trophic mode are displayed.

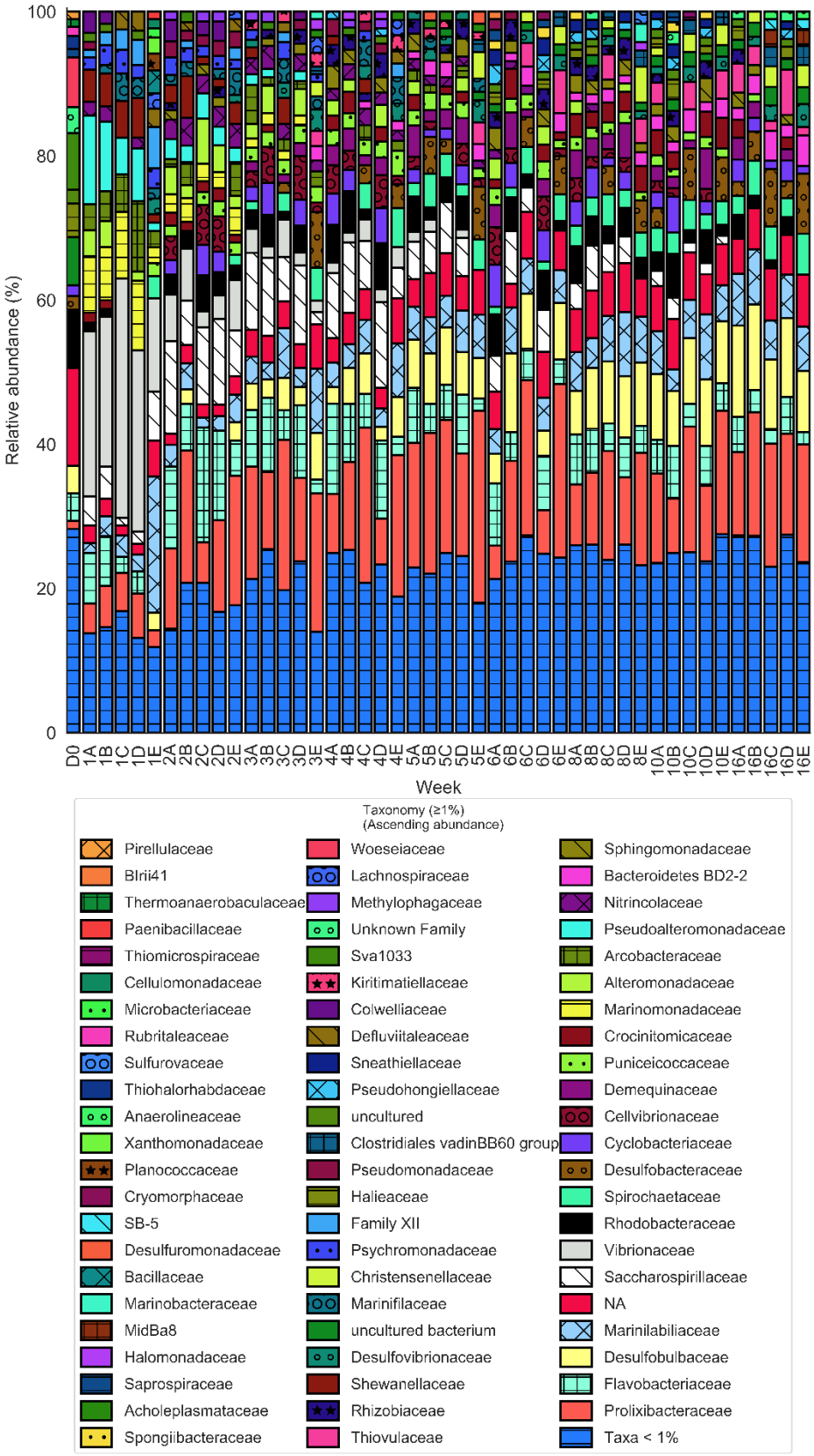


147

148 **Figure S13.** Bacteria profiles elucidated from 16S rRNA sequence homology, all biological replicates
149 are displayed at family level.

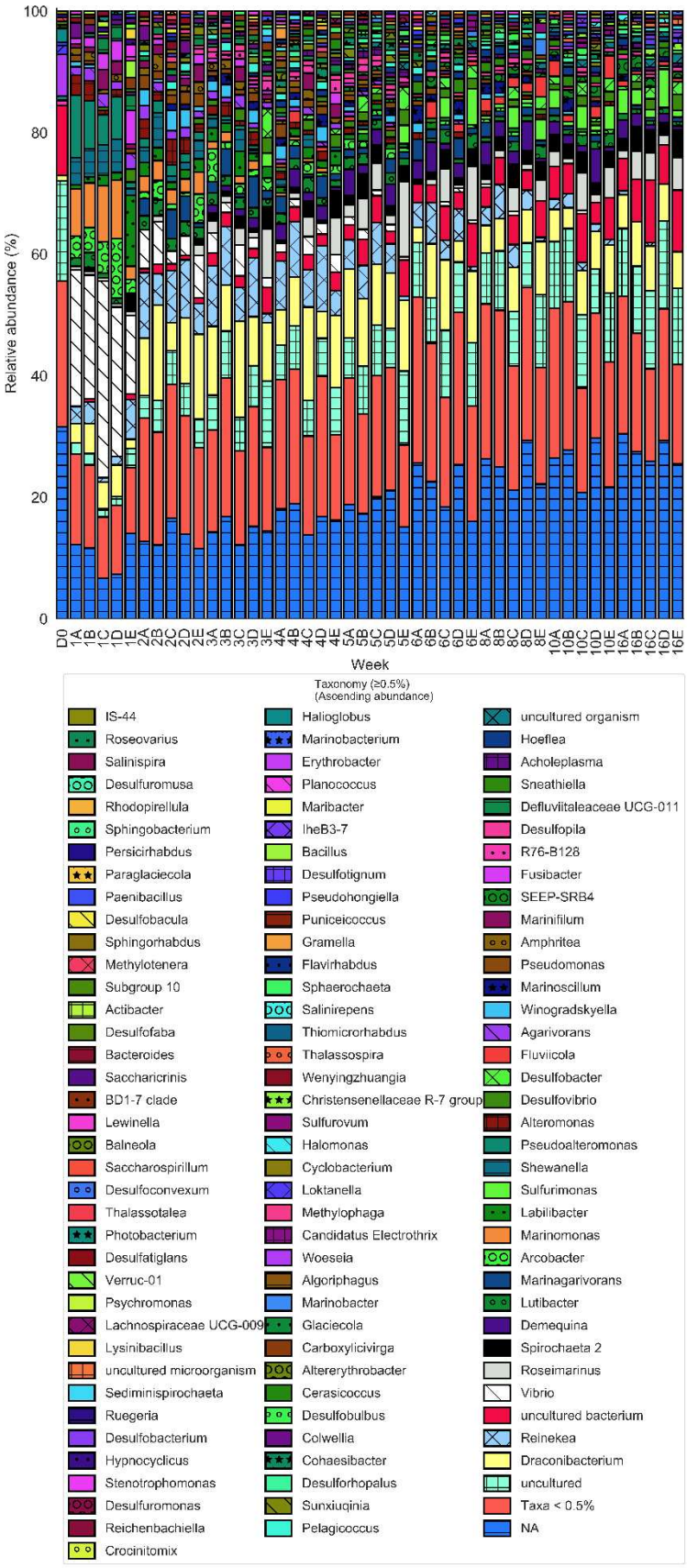


**Figure S14.** Bacteria profiles elucidated from 16S rRNA sequence homology, all biological replicates are displayed at genus level.

**Table S1.** Transect position of the five biological replicates in Welwick salt marsh. *OS GR*: ordnance survey grid reference.

| Cage | OS GR | Coordinates | Latitude/Longitude | Elevation (m) |
|---|---|---|---|---|
| **A** | TA 33850 18626 | 53.647022, 0.023465794 | 53°38'49.28"N/ 0° 1'24.48"E | 2 |
| **B** | TA 33915 18656 | 53.647271,0.024455525 | 53°38'50.18"N/ 0° 1'28.04"E | 2.2 |
| **C** | TA 33977 18676 | 53.647439, 0.025407313 | 53°38'50.78"N/ 0° 1'31.47"E | 2.7 |
| **D** | TA 34038 18704 | 53.647678,0.026343800 | 53°38'51.64"N/ 0° 1'34.84" | 3 |
| **E** | TA 34105 18719 | 53.647792, 0.027360971 | 53°38'52.05"N/ 0° 1'38.50"E | 3 |

† Coordinate accuracy ±4m

**Table S2.** Sequence reads throughout RNA sequence processing and assembly.

| | Week 1 | Week 3 | Week 5 | Week 10 | Total |
|---|---|---|---|---|---|
| Raw reads | 82 966 972 | 99 319 322 | 95 318 915 | 105 517 252 | 383 122 461 |
| Percentage reads rRNA | 10.71% | 1.58% | 2.74% | 2.04% | - |
| Paired end reads (-rRNA, -duplicates) | 68 307 441 | 91 948 286 | 85 685 871 | 93 709 355 | 339 650 953 |
| Paired end reads (-post QC) | 68 302 150 | 91 926 491 | 85 676 818 | 93 700 742 | 339 606 201 |
| Contigs (Trinity) | **4 100 865** | **9 720 697** | **7 501 904** | **8 615 202** | **29 938 668** |
| Genes (Trinity) | 3 869 004 | 9 132 509 | 7 071 997 | 8 153 028 | 28 226 538 |
| Median contig length (bp) | **187** | **195** | **185** | **201** | - |
| Average contig length (bp) | **268.28** | **247.46** | **255.67** | **249.49** | - |

**Table S3.** Commands for the replication of the 16S rRNA amplicon database processing pipeline. Emboldened characters are specific input or output files. Only steps utilising third party software is shown, custom steps are not shown. A1-A12 represent input or output files.

| Step | Function | Command |
|---|---|---|
| 1 | Merge | vsearch --fastq_mergepairs **X**1_001.fastq.gz --reverse **X**2_001.fastq.gz --fastqout **X**_16Smerged |
| 2A | Trim adapter | cutadapt -o nexteraremoved/**X** -a CTGTCTCTTATACACATCTGACGCTGCCGACGA **X** |
| 2B | Trim 13N | cutadapt --cut 13 -o **X X** |
| 3 | Fastq split | convert_fastaqual_fastq.py -c fastq_to_fastaqual -f **X** |
| 4 | Demultiplex | split_libraries.py -f **X** --max_ambig 0 -r -k -B -H 10 -M 2 -e 2 -b 7 -o **X** -m **MAP** |
| 5 | Trim primer | cutadapt --cut 19 --cut -20 -o **X X** |
| 6 | Concatenate | cat *.fna > catfile.fna |
| 7 | Format header | Format headers to >barcode label=sample_id;sequence_number_integer - custom |
| 8 | Global trim | usearch_v9 -fastx_truncate **A1** -trunclen 250 -fastaout **A2** |
| 9 | Dereplicate | usearch_v7 --derep_fulllength **A2** --output **A3** --log=log --sizeout --minuniquesize 2 |
| 10 | Sort by size | Usearch_v7 -sortbysize **A3** -output **A4** -minsize2 |
| 11 | Cluster | usearch_v9 -cluster_otus **A4**_cat16S.fna -otus **A5** -minsize 2 |
| 12 | Relabel | fasta_number.py **A5** OTU_>**A6** |
| 13 | Map OTUs | Usearch_v7 -usearch_global **A1** -db **A6** -strand plus -id 0.95 -uc A7 |
| 14 | Assign taxonomy | Assign_taxonomy.py -i **A6** -o **A8** --similarity 0.9 -r ref_set.fna -t ref_set.txt |
| 15 | OTU table (.txt) | uc2otutab.py **A7** > **A9**.txt |
| | | |
| 16* | .biom | Biom convert -I **A9** -o **A10** --table-type="OTU table" --to-hdf5 |
| 17* | .tsv | Biom convert -i **A10** -o **A11** --to-tsv |

*Optional

## References

1.Krzywinski M, Schein J, Birol I, Connors J, Gascoyne R, Horsman D, Jones SJ, Marra MA: Circos: An information aesthetic for comparative genomics. Genome Research. 2009; 19**:**1639-1645.
2.Kanehisa M, Sato Y, Morishima K: BlastKOALA and GhostKOALA: KEGG Tools for Functional Characterization of Genome and Metagenome Sequences. Journal of Molecular Biology. 2016;428:726-731.